# Point-by-Point Reply to Co-Editor of acp manuscript 2018-238 (author) – minor revisions

We thank the anonymous referee for his diligence regarding the second round of reviews of the above-referenced manuscript. We have carefully reread the entire manuscript, made corrections/additions here and there (highlighted in the track changes copy) and hope that we may satisfy the publication requirements as proposed in the following:

*Reviewer: I still feel that the introduction does not prepare the reader well enough for the results and discussion. On the one hand, the topic of acid dissociation is which covers more than a page of the manuscript is not at all taken up in the discussion. Even worse, taken that the atmospheric implications (5) discuss the lifetime of cloud particles this seems to be the central science tackled by the research. The introduction does not even once mention lifetime (except when giving goals of this paper) – I think you need to explain to the reader why this is important and which aspects are open concerning lifetime of ice particles in the atmosphere. In summary, the open questions around the water flux are still not clearly presented in the introduction, or lost in the details of the text, and the new aspects of this work relative to the previous publications could be more emphasized. However, I leave this decision to the editor.*

Author answer: We have tried to focus on two fundamental criteria regarding the occurrence of heterogeneous chemical reactions on atmospheric ices, namely (a) absolute evaporation rates of H2O in water-rich ices, and (b) elementary reaction kinetics of the interfacial processes yielding the precursors to atomic halogens.

Addition to text: Regarding heterogeneous chlorine activation leading to polar ozone loss in the LS (Solomon et al., 1986), but also tropical ozone depletion in the UT/LS region, there are two fundamental questions that continue to be raised, namely, (a) Do the involved heterogeneous reactions have sufficient time to proceed on the surface (interfacial chemical mechanism) or in the volume (bulk mechanism) of atmospheric ice particles? and (b) Are the heterogeneous reactions sufficiently rapid for the formation of the precursors of atomic chlorine under LS or UT/LS atmospheric conditions? Question (a) is directly related to the evaporative lifetime or the absolute rate of evaporation of $H_2O$, the main component of atmospheric ices, whereas (b) mainly depends on the chemical mechanism of the heterogeneous chlorine activation reaction and the ionic vs. molecular state of adsorbed HCl, either in the form of ionic hydrates ($H_3O^+(H_2O)_nCl^-$) or molecularly adsorbed HCl. Ionic reactions in a polar medium do not significantly slow down with lowering the temperature whereas reactions between closed shell molecules such as HCl and $ClONO_2$ or other molecules often have small barriers and thus are activated which leads to a significant decrease of the reaction rate with decreasing temperature. The present work primarily addresses the measurement of absolute rates of evaporation of $H_2O$ from atmospheric ices that therefore directly impact the lifetimes of

atmospheric ice particles under subsaturated atmospheric conditions. This enables the evaluation whether or not heterogeneous processing will take place to a significant extent taking into account published reports in the literature on the state of adsorbed HCl which is briefly summarized below.

*Reviewer: L 161 ff: "The question has to be raised whether the two types of used ice films may be responsible some of the discrepancies in the results because both the density and the structure of ice are known to be a strong function of temperature and deposition conditions (Kuhs et al., 2012; Schriver-Mazzuoli et al., 2000). This line gives the discussion of HCl dissociation a good reason with relevance to this work. I wonder, though, why the question of dissociation is not picked up in the discussion again taken that it occupies a rather large part of the introduction.*

Author Reply: By focusing on two fundamental criteria (see previous point) we create a link to the presentation of the adsorption state of HCl on ice. Question (a) (see previous) is treated in great detail in this work (evaporative lifetime), whereas question (b) is taken from literature results (adsorption state of HCl on ice). This is one of the reasons that we have not taken up this topic in the Discussion because we have not contributed to this subject in the present work although our FTIR spectra are consistent with the interpretation found in the literature.

No text added.

*Reviewer: L 199 ff: "It appears that two observed HCl species on/in ice, namely single phase amorphous $HCl/H_2O$ mixtures and a binary phase consisting of pure ice and an as yet unidentified crystalline HCl hydrate, $HCl•xH2O$, decrease $J_{ev}(H_2O)$ to a different extent as proposed in Delval et al. (2003)." Appear to me very close to the conclusions a, b, and e. May I ask you to stress the new findings in slight more detail.*

Author Reply: We are accommodating to the request of the reviewer by inserting the following text:

Text Addition: We believe that the unidentified crystalline HCl hydrate observed in Delval et al. (2003) corresponds to a metastable form of HCl hexahydrate because the bending vibration of the proton-ordered waters of hydration are split into a doublet (1644, 1618 $cm^{-1}$) in this work whereas all others report a single sharp peak in the range 1635 to 1643 $cm^{-1}$ (see Table 2 in Delval et al., 2003).

*Reviewer: L 288: The average mole fraction χHCl of HCl in the remaining ice film as a function of time is calculated according to Delval and Rossi (2005). Please detail on the method. Is this a direct measure of HCl deposited to the sample or rather indirect based on the gas-phase signal (dosage).*

Author Reply: We have entered the below-listed sentences into the text in order to briefly explain how the HCl mole fractions were determined.

Added text: Briefly, the number of HCl molecules adsorbed onto a given thin ice film consisting of a known number of $H_2O$ molecules using the calibrated signal of the QCMB has been established as a difference between the calibrated MS signals at m/e 36 of the quartz crystal sensor at ambient minus the (low) temperature of measurement akin to Figure 3 in Delval et al. 2005. Column 7 of Table 2 ($\mathbf{N}^{dep}_{HCl}$) displays the corresponding values. The HCl mole fraction $\chi^0_{HCl}$ has been established as the ratio $\mathbf{N}^{dep}_{HCl} / \mathbf{N}^{0}_{H2O}$ using the approximation $\mathbf{N}^{dep}_{HCl} << \mathbf{N}^{0}_{H2O}$ which is justified in this case as may be seen from the numbers displayed in column 4 and 7 of Table 2. This amounts to an absolute measurement of the number of HCl molecules lost or adsorbed onto the cold quartz sensor in contrast to a simple dose (exposure) measurement.

*Reviewer: Figure 2. Why are experiments 5 and 6 not discussed. Would this be a third type of ice?*

Author Reply: We clearly talk about limiting behavior of $J_{ev}(H_2O)$ by two defined states of HCl, namely crystalline HCl hydrate and amorphous $HCl/H_2O$ liquid. Experiments 5 and 6 seem to lie between these two limiting cases which makes the interpretation difficult. It may be an external or internal mixture of the crystalline and the amorphous phase, but we cannot say at the moment as we do not control the growth conditions.

*Reviewer: Figure 2. Why is experiment 10 not shown even thought it is discussed in the text? Please add.*

Author Reply: Experiment 10 is presented in Table 2. The reason we have not included it in Figure 2 is that it is not particularly compelling. It just makes the drawing even more crowded such that we decided to omit it from the graph as it does not confer any new information.

# The Influence of HCl on the Evaporation Rates of $H_2O$ over Water Ice in the Range 188 to 210 K at small Average Concentrations

Christophe Delval[1,2,a] and Michel J. Rossi[1,3]

[1]Laboratory of Air and Soil Pollution Studies (LPAS), ENAC Faculty, Swiss Federal Institute of Technology (EPFL), CH-1015 Lausanne, Switzerland

[2]Atmospheric Particle Research Laboratory (APRL), ENAC Faculty, Swiss Federal Institute of Technology (EPFL), CH-1015 Lausanne, Switzerland

[3]Laboratory of Atmospheric Chemistry (LAC), Paul Scherrer Institute (PSI), CH-5232 Villigen-PSI, Switzerland

[a]Present Address: Patent Examiner - Directorate 1657, Dir. 1.6.5.7, European Patent Office, Patentlaan 3-9, 2288 EE Rijswijk, Netherlands

Corresponding author: michel.rossi@psi.ch

## ABSTRACT

The evaporation flux $J_{ev}(H_2O)$ of $H_2O$ from HCl-doped typically 1.5 μm or so thick vapor-deposited ice films has been measured in a combined quartz crystal microbalance (QCMB) – residual gas mass spectrometry (MS) experiment using a stirred flow reactor (SFR). $J_{ev}(H_2O)$ has been found to show complex behaviour and to be a function of the average mole fraction $\chi_{HCl}$ of HCl in the ice film ranging from $6x10^{14}$ to $3x10^{17}$ molecule $cm^{-2}$ $s^{-1}$ at 174 – 210 K for initial values $\chi^0_{HCl}$ ranging from $5x10^{-5}$ to $3x10^{-3}$ at the start of the evaporation. The dose of HCl on ice was in the range of 1 to 40 formal monolayers and the $H_2O$ vapor pressure was independent of $\chi_{HCl}$ within the measured range and equal to that of pure ice down to 80 nm thickness. The dependence of $J_{ev}(H_2O)$ with increasing average $\chi_{HCl}$ was correlated with (a) the evaporation range $r^{b/e}$ parameter, that is the ratio of $J_{ev}(H_2O)$ just before HCl-doping of the pure ice film and $J_{ev}(H_2O)$ once most of HCl has desorbed towards the end of film evaporation, and (b) the remaining thickness $d_D$ below which $J_{ev}(H_2O)$ decreases to less than 85% of pure ice. The dependence of $J_{ev}(H_2O)$ with increasing average $\chi_{HCl}$ from HCl-doped ice films suggests two limiting data sets: One consisting of a two-phase pure ice/crystalline HCl hydrate binary phase (set A), and the other of a single phase amorphous $HCl/H_2O$ binary mixture (set B). The measured values of $J_{ev}(H_2O)$ may lead to significant evaporative life-time extensions of HCl-contaminated ice cloud particles under atmospheric conditions, regardless of whether the structure corresponds to an amorphous or crystalline state of the $HCl/H_2O$ aggregate.

Deleted: after observable

Deleted: ption

Deleted: ,

Deleted: o

Deleted: associated with the occurrence of

Deleted: with

## 1. INTRODUCTION

HCl is among the mineral acids that control the acidity of the atmosphere together with $HNO_3$ and $H_2SO_4$. The production of atmospheric HCl is predominantly taking place in the middle and upper stratosphere where $O_3$ is formed owing to photolysis of halogen containing source gases such as CFC's (chlorofluorocarbons). However, there are no known sources of HCl in the upper troposphere (UT) because scavenging processes of HCl throughout the troposphere are very efficient which leads to HCl background concentrations of less than 0.1 ppb (Graedel and Keene, 1995). The absence of significant sources in the troposphere, the long photolytic lifetime of HCl and the fact that the production region is well separated from the regions of interest, namely the UT and the lower stratosphere (LS) all contribute to the fact that HCl is an excellent tracer for stratospheric ozone in the UT (Marcy et al., 2004). Owing to the frequent occurrence of Cirrus clouds in this atmospheric region it is of obvious interest to study the interaction of HCl with atmospheric ice particles at relevant temperature and pressure conditions (Jensen et al. 2001; Zerefos et al., 2003). The compact correlation between $O_3$ and HCl has been used to monitor stratospheric-tropospheric exchange processes and stratospheric $O_3$ intrusions into the troposphere that are still an active field of investigation (Houghton et al., 2001).

HCl is of importance in the LS as it partakes in heterogeneous reactions on Polar Stratospheric Clouds (PSC's consisting either of nitric acid trihydrate, $HNO_3 \cdot 3H_2O$ or Cirrus clouds), on Cirrus clouds in the UT/LS region (Borrmann et al., 1996) as well as on background stratospheric $H_2SO_4$ aerosol according to the following reaction taken as an example of the many possible heterogeneous processes:

$$HCl(ads) + ClONO_2 \rightarrow Cl_2(g) + HNO_3(ads)$$

These reactions efficiently convert inactive Cl-containing reservoir molecules such as HCl and $ClONO_2$ into active photolyzable Cl-containing compounds in a single reaction. Typical examples of such photolabile reaction products are $Cl_2$, $ClNO_2$ and HOCl that will change the atmospheric composition owing to the high reactivity of the photolysis products such as atomic Cl (Solomon et al., 1986; Tolbert et al., 1987; WMO 2003). It thus follows that HCl is of stratospheric (LS) importance and is frequently used as a model compound for heterogeneous chlorine activation reactions on ices that has inspired many laboratory kinetic studies (Leu et al., 1991; Hanson and Ravishankara, 1992; Chu et al., 1993; Flückiger et al., 1998; Hynes et al., 2001; Abbatt, 2003).

Deleted: Ice

Formatted: Subscript

Formatted: Subscript

Regarding heterogeneous chlorine activation leading to polar ozone loss in the LS (Solomon et al., 1986), but also ozone depletion in the tropical UT/LS region, there are two fundamental questions that continue to be raised, namely, (a) Do the involved heterogeneous reactions have sufficient time to proceed on the surface (interfacial chemical mechanism) or in the volume (bulk mechanism) of atmospheric ice particles? and (b) Are the heterogeneous reactions sufficiently rapid for the formation of the precursors of atomic chlorine under LS or UT/LS atmospheric conditions? Question (a) is directly related to the evaporative lifetime or the absolute rate of evaporation of $H_2O$, the main component of atmospheric ices, whereas (b) mainly depends on the chemical mechanism of the heterogeneous chlorine activation reaction and the ionic vs. molecular state of adsorbed HCl, either in the form of ionic hydrates ($H_3O^+(H_2O)_nCl^-$) or molecularly adsorbed HCl. Ionic reactions in a polar medium do not significantly slow down with lowering the temperature whereas reactions between closed shell molecules such as HCl and $ClONO_2$ or other molecules often have small barriers and thus are activated which leads to a significant decrease of the reaction rate with decreasing temperature. The present work primarily addresses the measurement of absolute rates of evaporation of $H_2O$ from atmospheric ices that therefore directly impact the lifetimes of atmospheric ice particles under subsaturated atmospheric conditions. This enables the evaluation whether or not heterogeneous processing will take place to a significant extent taking into account published reports in the literature on the state of adsorbed HCl which is briefly summarized below.

HCl forms hydrates of variable stoichiometry when exposed to ice depending on the temperature of deposition and the partial pressure of HCl (Ortega et al., 2004; Graham and Roberts, 1997). X-Ray diffraction has allowed the identification of four crystalline hydrates containing one (Yoon and Carpenter, 1959), two (Lundgren and Olovson, 1967), three (Lundgren and Olovson, 1967a) and six (Taesler and Lundgren, 1978) $H_2O$ per HCl molecule. In addition, amorphous mono-, tetra- and hexahydrates have been reported under various experimental conditions (Yoon and Carpenter, 1959; Delzeit et al., 1993). The control of growth conditions of a specific HCl hydrate is sometimes elusive, but the formation of a saturated HCl hexahydrate phase has been reported at sufficiently large HCl exposure (Graham and Roberts, 1995) using amorphous ice as a starting point despite the fact that the hexahydrate is said to nucleate with difficulty, at least in thin films (Ortega et al., 2004). However, the molecular and dynamic details of the crystallization process have not been investigated as yet.

Formatted: Indent: First line: 1,25 cm
Deleted: tropical
Formatted: Subscript
Formatted: Subscript
Formatted: Superscript
Formatted: Subscript
Formatted: Subscript
Formatted: Superscript
Formatted: Subscript
Formatted: Subscript

Fourier-Transform IR (FTIR) absorption measurements have enabled the characterization of both amorphous as well as crystalline HCl hydrates at growth conditions that are sometimes significantly different compared to the samples investigated using X-Ray diffraction. Vibrational spectra of HCl hydrates in the mid IR have been routinely used for identification purposes for some time (Ferriso and Hornig, 1955; Gilbert and Sheppard, 1973). Recently, the mid IR absorption spectra of the four HCl hydrates mentioned above have been assigned in a comprehensive and definitive way, albeit without simultaneous proof of the crystalline structure using X-Ray diffraction (Buch et al., 2002; Xueref and Dominé, 2003). More recently, the reflection absorption IR spectrum (RAIR) of crystalline HCl hexahydrate in the mid-IR range has been recorded and assigned using theoretical calculations based on density functional theory that results in a refinement of the geometric structure of the HCl hydrates and a prediction of the vibrational modes of the crystal (Ortega et al., 2004). It must be recalled that FTIR spectra in transmission and reflection may in most cases not be directly compared across the mid IR range.

Regarding the nature of the HCl-ice adsorbate one of the important questions is whether adsorbed HCl is ionized or exists as a molecular adsorbate under atmospherically relevant conditions of the UT/LS. This will determine the mechanism of the heterogeneous reaction which constitutes necessary knowledge for the extrapolation of heterogeneous reaction rates measured in the laboratory to real atmospheric conditions. Thermal desorption of HCl monitored by IR absorption in the mid-IR range revealed a molecularly adsorbed state of HCl desorbing below 50 K (Delzeit et al., 1993a). IR studies performed by Banham et al. on HCl-ice films failed to detect molecularly adsorbed HCl at $T \geq 90$ K despite the high rate of HCl adsorption in that temperature range (Banham et al., 1995). In contrast, Graham and Roberts attributed a characteristic Temperature Programmed Desorption (TPD) peak of a HCl/amorphous ice adsorbate monitored by residual gas MS and occurring at 150 K to molecularly adsorbed HCl (Graham and Roberts, 1995). However, they did not report the IR absorption spectrum of the adsorbate in the mid-IR nor did they explain why molecular adsorption of HCl exclusively occurred on amorphous, but not on crystalline ice. Most recent results seem to point towards the existence of molecularly adsorbed HCl on ice below 50 K and at submonolayer coverages in coexistence with ionized solvated HCl whose fraction increases with increasing ice temperature (Buch et al., 2002; Delzeit et al, 1993a; Delzeit et al. 1997; Uras et al., 1998; Devlin et al., 2002; Lu and Sanche, 2001). Kang et al. discovered that both molecularly adsorbed as well as ionized HCl coexisted on ice that was deposited

under Ultra-High Vacuum (UHV) conditions in the temperature range 50 to 140 K and under conditions of low HCl exposure (Kang et al., 2000).

Although theoretical electronic structure calculations predict spontaneous ionization of adsorbed HCl (Gertner and Hynes, 1996; Bolton and Petterson, 2001) most experiments point towards a seemingly thermally activated ionization process that may be enabled by structural factors of the ice matrix that are themselves a function of temperature. Consistent with these results concentration profiling experiments of HCl/ice adsorbates using static Secondary Ionization Mass Spectroscopy (SIMS) techniques failed to discover molecularly adsorbed HCl on ice in the range 90-150 K (Donsig and Vickerman, 1997). In conclusion, both experimental and theoretical studies clearly point to the absence of significant quantities of molecularly or covalently adsorbed HCl under stratospheric conditions. Instead, HCl is ionized and solvated by $H_2O$ on the surface of ice films and may occur either as amorphous $HCl/H_2O$ hydrates of undefined stoichiometry or as crystalline HCl hydrates. However, these facts do not rule out the presence of small amounts of molecularly adsorbed HCl on ice that may be intermediates in the complex mechanism of HCl adsorption on ice as evidenced by the negative temperature dependence of the rate of uptake of HCl on ice (Flückiger et al., 1998). In fact, such an intermediate has been invoked in the description of HCl adsorption on ice under atmospheric conditions using a chemical kinetic model based on a multitude of experimental observables collected upon HCl uptake on ice (Flückiger and Rossi, 2003).

Work by Parent and coworkers uses Near-Edge X-Ray Absorption Spectroscopy (NEXAFS) of HCl-doped low temperature ice substrates in order to determine the relative population of ionic and covalently bound HCl and distinguish between bulk and HCl surface states in the temperature range 20 to 150 K (Bournel et al., 2002; Parent and Laffon, 2005). The results seem to confirm the consensus on the low-temperature existence of molecularly adsorbed HCl up to 90 K beyond which an increasing amount of HCl is converted into an ionic form, such as $H_3O^+Cl^-$ (Eigen cation) or $H_5O_2^+Cl^-$ (Zundel cation) formed by spontaneous ionization of adsorbed HCl on ice, up to completion at 150 K (Buch et al., 2008). The newest work by Parent compares NEXAFS with photoemission (UPS, XPS) and FTIR in transmission of thin $HCl/H_2O$ films (Parent et al., 2011). The results are roughly consistent but surprising in the sense that these workers find 92% ionically dissolved HCl in/on ice at 50 K in contrast to Kang et al. (2000) and Devlin et al. (2000) under similar exposure (dose) and temperature conditions. In addition, Parent et al. (2011) performed the NEXAFS experiment on a (thick) 100 ML "crystalline" $H_2O$ ice substrate deposited at 150 K whereas the photoemission and FTIR absorption experiments used a 4 ML thin ice slab deposited at 120

K. The question has to be raised whether the two types of used ice films may be responsible for some of the discrepancies in the results because both the density and the structure of ice are known to be a strong function of temperature and deposition conditions (Kuhs et al., 2012; Schriver-Mazzuoli et al., 2000). The most recent work of Parent et al. (2011) sparked an interesting controversy in the assignment of the FTIR absorption spectrum of thin HCl/$H_2O$ films and led to two comments showcasing the difficulties of intercomparison of nominally identical experiments (Devlin and Kang, 2012; Parent et al., 2012).

Furthermore, the results indicate that the "dangling bonds" of the ice surface attributed to isolated OH groups are not the unique site of HCl adsorption, even in the range 20-90 K (Flückiger and Delval, 2002). The present work suggests that maiden uptake of HCl onto pure ice weakens and perturbs the crystal structure of the ice matrix in an irreversible way such that additional sites for HCl adsorption and ionization are created akin to Parent et al. (2011). Initial HCl uptake on pure ice therefore has a catalytic effect on the following HCl uptake. This irreversible nature of initial HCl dosing has been known for several years and been observed some time ago in Knudsen flow reactor studies on the HCl/$H_2O$ system under steady-state conditions of both HCl and $H_2O$ at temperatures representative of the UT/LS (Flückiger et al., 1998; Oppliger et al., 1997). The most recent experimental work on HCl/$H_2O$ at an atmospherically relevant ("warm") temperature (253 K) has examined the HCl depth profile using XPS spectroscopy and finds molecularly adsorbed (physisorbed) HCl at its outermost layer and ionic dissociation in deeper layers (Kong et al., 2017). Complementary X-Ray absorption results also point towards a perturbation of the crystal structure of ice in the aftermath of HCl adsorption/dissolution into deeper layers of ice.

We have concluded from recent work that HCl doping in quantities of submonolayer to several monolayers of HCl leads to the decrease of both the evaporative flux $J_{ev}$ (molecule $cm^{-2}s^{-1}$) or rate $R_{ev}$ (molecule $cm^{-3}s^{-1}$) and the rate of condensation $k_{cond}$ ($s^{-1}$), of $H_2O$ in the presence of ice *without* perturbing the equilibrium vapour pressure of $H_2O$, $P_{H2O}^{eq}$ (Delval et al., 2003). We have furthermore shown that the way $J_{ev}$ of $H_2O$ decreases with time depends on the rate of deposition or the integral of deposited HCl, namely $R_{HCl}$ (molecule $s^{-1}$) and $N_{HCl}$ (molecule), respectively. It appears that two observed HCl species on/in ice, namely single phase amorphous HCl/$H_2O$ mixtures and a binary phase consisting of pure ice and an as yet unidentified crystalline HCl hydrate, HCl•x$H_2O$, decrease $J_{ev}(H_2O)$ to different extents as proposed in Delval et al. (2003). We believe that the unidentified crystalline HCl hydrate observed in Delval et al. (2003) corresponds to a metastable form of HCl hexahydrate because the bending vibration of the proton-ordered waters of hydration are split into a doublet (1644,

Deleted: is

Deleted: has

Formatted: Font: Italic

Deleted: a

1618 $cm^{-1}$) in this work whereas all others report a single sharp peak in the range 1635 to 1643 $cm^{-1}$ (see Table 2 in Delval et al., 2003). These results have led us to perform systematic experiments in this work using the Quartz Crystal MicroBalance (QCMB) combined with residual gas Mass Spectrometry (MS) that we have used successfully in the past (Delval and Rossi, 2004) in order to investigate the temporal change of $J_{ev}(H_2O)$ with increasing average mole fraction of HCl, $\chi_{HCl}$, remaining in the ice. One of the goals of the present work is to determine the influence of the HCl deposition parameters on the temporal change of $J_{ev}$ and the mass accommodation coefficient $\alpha$ during evaporation of a HCl-doped ice film and its consequence on the lifetime of atmospheric ice particles contaminated by HCl. This issue is key in relation to the importance of heterogeneous vs. homogeneous atmospheric reactions at midlatitudes as has been pointed out in the past (Solomon et al., 1986; 1997).

## 2. EXPERIMENTAL

The emphasis of the present experiments was placed on the deposition of small amounts of HCl ranging in doses from 1 to 40 formal monolayers of HCl where a formal monolayer of adsorbed HCl corresponded to a surface concentration of $2.5x10^{14}$ molecule $cm^{-2}$ (Table A1) which is a consensus value obtained from several selected experiments. The apparatus as well as the methods used for calibration and the HCl deposition procedure have been described in detail elsewhere using $HNO_3$ as a case in point (Delval and Rossi, 2005). The experimental conditions are generally identical to the ones presented in Delval and Rossi (2005) and the instrumental parameters are summarized in Table 1. The only significant difference between the study of $HNO_3$-doped ice and the present condensed phase investigation of HCl-doped ice lies in the mode of trace gas admission. HCl was deposited by backfilling the reactor under stirred flow reactor (SFR) conditions with the inlet tubing used for trace gas injection oriented towards one side of the Si-window of the cryostat set at ambient temperature whereas $HNO_3$ was deposited by directed injection onto ice films supported by the quartz crystal of the QCMB as referenced above in order to minimize the interaction of $HNO_3$ with the internal surfaces of the SFR at ambient temperature which leads to nitric acid decomposition. Evaporation experiments have been performed isothermally on samples in the temperature range 174-210 K under dynamic pumping conditions, that is at maximum pumping speed (gate valve open) in order to prevent readsorption of HCl on the ice substrate under molecular flow conditions.

Formatted: Superscript

Formatted: Superscript

Deleted: the

Formatted: Subscript

Formatted: Subscript

First, an approximately 1.5 μm thick ice film was grown at 190 K on the quartz crystal of the QCMB by deposition of bidistilled water vapor at a rate of $1x10^{17}$ molecule $cm^{-2}$ $s^{-1}$ under static conditions. The $H_2O$ equilibrium vapor pressure agreed with published values across the covered temperature range (Marti and Mauersberger, 1993; Mauersberger and Krankowsky, 2003). Subsequently, the system was set to the desired temperature given in Table 2 (second column from the left) and a metered amount of HCl was deposited under stirred flow conditions. The rate of deposition of HCl, $R_{HCl}$, as well as its time integral, namely the number of HCl molecules deposited on ice, $N_{HCl}$, have been evaluated using the method described in Delval and Rossi (2005). Typically, $R_{HCl}$ ranges between $8.0x10^{11}$ and $4.2x10^{13}$ molecule $s^{-1}$ and $N_{HCl}$ between $1.0x10^{14}$ and $5.4x10^{15}$ molecules. The experimental conditions of HCl-deposition as well as important experimental parameters are reported in Table 2. Finally, the system was set to dynamic pumping conditions by opening the gate valve to the turbopump. $J_{ev}(H_2O)$ was measured isothermally using both the QCBM and residual gas MS. Figure 1 illustrates a typical experimental protocol of the evaporation at 192 K of a HCl-doped ice film labelled as experiment 11 in Table 2 and performed as a multidiagnostic experiment where both the gas- as well as the condensed phases are simultaneously monitored.

At t = 0 ($t_0$), the system is set from stirred flow to dynamic pumping that starts the evaporation experiment. The continuous curve marked with the empty squares symbol in Figure 1A corresponds to $J^{QCM}_{ev}$, the evaporative flux of $H_2O$ calculated from the raw signal at the output of the QCMB. The diamond symbol (◊) corresponds to $J^{18}_{ev}$ evaluated from $I^{18}$, the MS signal amplitude for $H_2O$ monitored at m/e = 18. Int($J^{18}_{ev}$) marked by triangles in Figure 1A is the time integral of $J^{18}_{ev}$ and corresponds to the total number of $H_2O$ molecules that have evaporated from the ice film at t. D is the label at time $t_D$ at which $J_{ev}(H_2O)$ decreased from its original value corresponding to pure ice to 85% of its original value at t = 0, and $d_D$ is the remaining thickness of the ice film at $t_D$. $H_b$ and $H_e$ in Figure 1B correspond to the time when HCl evaporation begins and ceases to be observed, respectively, using gas phase residual mass spectrometry (x symbols in Figure 1B) and are labeled $t_{Hb}$ and $t_{He}$. The data have been treated in analogy to $HNO_3$-doped ice through the formalism given in Delval and Rossi (2005). Akin to $HNO_3$ the mass balance between HCl deposited, $N^{dep}_{HCl}$, and HCl recovered during ice evaporation, $N^{evap}_{HCl}$, agrees to within less than a factor of 2 under dynamic pumping conditions. We therefore estimate the average uncertainty (2σ) of the HCl mole fraction $\chi_{HCl}$ of ± 18 % from the average discrepancy between $N^{dep}_{HCl}$ and $N^{evap}_{HCl}$ displayed

Formatted: Subscript

in Table 2. In the following $N_{HCl}$ will always refer to $N^{dep}_{HCl}$ derived from the measurement of HCl at deposition because it is related to a directly measured quantity originating from a measured pressure decrease in a given volume and time interval $\Delta P/\Delta t$. The present experiments cover the evaporation of a small albeit important fraction of the model ice film for which the decrease of $J_{ev}(H_2O)$ is significant.

## 3. RESULTS

The experimental data reported in Table 2 on the isothermal change of the evaporative flux of water, $J_{ev}(H_2O)$, as a function of the average mole fraction of HCl, $\chi_{HCl}$, in the remaining ice film during the evaporation process under dynamic conditions are presented in Figure 2. Dynamic pumping conditions ensure the absence of any readsorption of $H_2O$ vapor during evaporation owing to the low $H_2O$ partial pressures in the reactor. The axes labelled "b" and "e" correspond to the values of $J_{ev}(H_2O)$ at the end of ice film deposition and after desorption of most of the adsorbed HCl from the HCl-doped ice film at $t_{He}$, respectively, as displayed in Figure 1B. The average mole fraction $\chi_{HCl}$ of HCl in the remaining ice film as a function of time is calculated according to Delval and Rossi (2005). Briefly, the number of HCl molecules adsorbed onto a given thin ice film consisting of a known number of $H_2O$ molecules using the calibrated signal of the QCMB has been established as a difference between the calibrated MS signals at m/e 36 of the quartz crystal sensor at ambient minus the (low) temperature of measurement akin to Figure 3 in Delval et al. 2005. Column 7 of Table 2 ($N^{dep}_{HCl}$) displays the corresponding values. The HCl mole fraction $\chi^0_{HCl}$ has been established as the ratio $N^{dep}_{HCl} / N^0_{H2O}$ using the approximation $N^{dep}_{HCl} << N^0_{H2O}$ which is justified in this case as may be seen from the numbers displayed in column 4 and 7 of Table 2. This amounts to an absolute measurement of the number of HCl molecules lost or adsorbed onto the cold quartz sensor in contrast to a simple dose (exposure) measurement where one does not know the amount of adsorbed molecules.

The change in $\chi_{HCl}$ owing to $H_2O$ evaporation is evaluated between $t = t_D$ and $t = t_{Hb}$ that corresponds to the time interval when the number of adsorbed HCl molecules is constant as no release of HCl is observable in the gas phase at m/e = 36 before $t_{Hb}$. Table 2 also displays the initial value of the HCl mole fraction, $\chi^0_{HCl}$, calculated for the ice film just at the end of HCl deposition and marked by a colored circle on the experimental trajectory of a color-coded evaporating ice film displayed in Figure 2. The average mole fraction of HCl in

Deleted: refers

Formatted: Subscript

the ice film, $\chi_{HCl}$, increases owing to evaporation of $H_2O$ from the ice film without loss of HCl such that the elapsed time of the $H_2O$ evaporation experiment increases with $\chi_{HCl}$ in Figure 2.

The beginning of an evaporation experiment after the end of HCl doping (t = 0 in Figure 1 or $t_0$ in Figure 2) is marked by a colored circle of a given experiment whose parameters are displayed in Table 2 and Figure 2 (see experiment 8). As pointed out above, at $t = t_D$ $J_{ev}(H_2O)$ has decreased to an arbitrarily chosen value of 85% of its original value measured at $t = t_0$ that corresponds to the beginning of the bold color-coded smooth curve of a given experiment. Figure 2 essentially displays trajectories of evaporation experiments from $t_0$ (colored circle) moving to $t_D$ and finishing at $t_{Hb}$ between the two limiting values for pure ice (color coded number of a given experiment on axis "b" for "beginning") and the remaining ice film at the end of measurable HCl desorption $t_{He}$ (color-coded number of experiment on axis "e" for "Halogen end"). The trajectory of an experiment with values of $\chi_{HCl}$ between $t_0$ (colored circle at $\chi^0_{HCl}$) and $t_D$ (beginning of bold colored line, see experiment 8 in Figure 2) ending at $t_{Hb}$ (end of bold line, experiment 8) is presented as a bold dashed-dotted and bold smooth line from $t_0$ to $t_{Hb}$, respectively, in order to emphasize the quantitative portion of the experiment. Thinner (color-coded) dotted lines connect the end of ice film deposition (colored circle on axis "b") and HCl-dosing with $t_0$, the beginning of the evaporation experiment and also describe the post-phase of evaporation starting at $t_{Hb}$ to $t_{He}$ in order to guide the eye of the reader to imagine a complete evaporation cycle.

Two limiting cases of data sets of the change of $J_{ev}(H_2O)$ with $\chi_{HCl}$ may be distinguished in Figure 2. The first kind of data set corresponds to the curves describing $J_{ev}$ for experiments 1, 2, 9 and 11 and is called dataset A. These traces present a slow continuous decrease of $J_{ev}(H_2O)$ as $\chi_{HCl}$ increases during $H_2O$ evaporation. The second type of dataset shows an initial plateau of $J_{ev}(H_2O)$ with increasing $\chi_{HCl}$ starting at the value of pure ice evaporation followed by a sudden decrease of $J_{ev}(H_2O)$ and is found for experiments 3, 4, 7 and 8 which we call dataset B. Akin to $HNO_3$, we have evaluated the impact of the HCl deposition protocol on the evaporation range parameter, $r^{b/e}$, which is the ratio between the evaporative flux of $H_2O$ at the beginning of ice evaporation, $J^b_{ev}(H_2O)$ reported on the left axis "b" in Figure 2, and $J_{ev}(H_2O)$ close to the end of the desorption of HCl, $J^e_{ev}(H_2O)$, at $t = t_{He}$ (the right axis "e" in Figure 2). It describes the ratio by which $J_{ev}(H_2O)$ decreases within the limits of "b" and "e". The impact of both the rate of deposition of HCl on ice, $R_{HCl}$, and its time integral corresponding to the dose of deposited HCl, $N_{HCl}$, are presented in Figures 3 and Figure A1 (Appendix), respectively.

Formatted: Subscript

Deleted: different

Deleted: factor

459 It appears from these Figures that we have not succeeded to find a simple experimental
460 parameter that controls $J_{ev}(H_2O)$ either with elapsed time or amount of adsorbed HCl
461 expressed as the time dependence of $\chi_{HCl}$. Instead, the data may roughly be classified along
462 the two cases presented above, namely datasets A and B. The distinction between both data
463 sets seems to be the rate of change (slope) of $J_{ev}(H_2O)$ within a fairly narrow range of $\chi_{HCl}$.
464 Indeed, the available number of experiments clearly shows two distinct and limiting cases
465 whereas the search for other controlling parameters such as $R_{HCl}$, $N_{HCl}$ and the temperature of
466 deposition ($T_{ice}$) for dataset A failed akin to a similar study of $HNO_3$ (Delval and Rossi,
467 2005).
468 One may take note for instance of the low value of $\chi_{HCl}$ at 210 K for experiment 9
469 where the conditions of deposition are similar to experiments 1 and 2, yet, its respective
470 values of $r^{b/e}$ differ significantly from experiment 9 (Figure 3). In contrast, for dataset B the
471 $r^{b/e}$ values are similar for the whole set and range from 20 to 27.2 staying within a fairly
472 narrow band. Moreover, they seem to be independent of $R_{HCl}$ and $N_{HCl}$ as for data set A. In
473 contrast, the $r^{b/e}$ values for dataset A seem widely scattered over the explored parameter space.
474 We have also investigated the impact of the deposition protocol on $d_D$, which is the thickness
475 of ice that is affected by the presence of HCl, namely the remaining thickness of ice whose
476 $J_{ev}(H_2O)$ value has decreased to 85% of $J_{ev}(H_2O)$ of pure ice. The results on $d_D$ as a function
477 of $R_{HCl}$ and $N^{dep}_{HCl}$ are presented in Figures 4 and A2 (Appendix), respectively. Taking the
478 results of Figures 3, 4, A1 and A2 together we arrive at the following two conclusions:
479 (1) $T_{ice}$, $R_{HCl}$ and $N^{dep}_{HCl}$ are not controlling parameters or predictors for the dependence of
480 $J_{ev}(H_2O)$ as a function of $\chi_{HCl}$ in either set.
481 (2) The evaporation range parameters $r^{b/e}$ and $d_D$ are not characterizing set A. In contrast, for
482 dataset B, $r^{b/e}$ and $d_D$ values fall into a narrow range with values varying from 460.7 to 636.0
483 nm compared to the original ice thickness $d_0$ of 1'500 nm or so (exact numbers may be found
484 in Table 2).
485
486 **4. DISCUSSION**
487
488 Figure 1 displays the evaporation history of sample 11 as an example whose deposition
489 parameters are listed in Table 1. The initial average mole fraction $\chi_{HCl}^0$ of HCl, once
490 deposition on the 1.44 μm thick ice film under stirred flow reactor conditions is terminated,
491 has been estimated from the total number of $H_2O$ molecules contained in the ice film and the
492 measured number of deposited HCl molecules, $N^{dep}_{HCl}$, for experiment 11 (Table 2). Table 2

Deleted: study

Deleted: of

and Figure 1 reveal that for approximately $2.2x10^{18}$ $H_2O$ molecules in the film and $5.4x10^{14}$ molecules of deposited HCl, we obtain $\chi_{HCl}^0 = 2.7x10^{-4}$. This HCl mole fraction represents an average value that takes into account all $H_2O$ molecules contained in the ice film whereas in reality there will be a HCl gradient across the ice film as has been observed in the case of the $HNO_3$/ice system (Delval and Rossi, 2005). However, the present experiments are unable to determine the HCl concentration gradient (profile) across the interface.

After the HCl deposition process on the typically 1.5 μm thick ice film the gate valve is opened in order to initiate the isothermal evaporation experiment under dynamic pumping conditions. Initially, $H_2O$ evaporates at fluxes $J_{ev}(H_2O)$ that are characteristic of pure ice measured previously (Delval and Rossi, 2004; Pratte et al., 2006). These initial values $J_{ev}^b(H_2O)$ are displayed on the left-hand "b" (= "beginning") axis in Figure 2. As the evaporation proceeds $J_{ev}(H_2O)$ slightly decreases with time as displayed in Figure 1A to the arbitrarily chosen point where $J_{ev}(H_2O)$ has decreased to 85% of the initial pure ice value at which point the remaining ice thickness $d_D$ has decreased by approximately one third to 771.7 nm remaining ice thickness as displayed in Figure 1B and Table 2. Further evaporation of $H_2O$ leads to a continuous decrease of $J_{ev}(H_2O)$ at a corresponding increase of $\chi_{HCl}$ up to point $H_b$ defined above ("Halogen beginning") at $t_{Hb}$ (Figure 1B) where HCl starts to desorb from the ice film as monitored using the residual MS signal at m/e = 36.

For $t < t_{Hb}$, $\chi_{HCl}$ is given by the number of originally deposited HCl molecules that remain adsorbed on the ice film up to $t_{Hb}$ and the remaining $H_2O$ molecules in the film. In contrast, for $t > t_{Hb}$ the composition of the remaining ice film must be determined by taking into account the loss by evaporation of both $H_2O$ and HCl. The present experimental configuration is not adapted to simultaneously measure HCl loss. Therefore, we have chosen to display the temporal development of $J_{ev}(H_2O)$ for $t < t_{Hb}$ in Figure 2 as a function of the average value of the HCl mole fraction $\chi_{HCl}$. However, the value of $J_{ev}(H_2O)$ at $t = t_{He}$ where most of the HCl has desorbed from the ice film is plotted on the right axis labelled "e" (= "end") as $J_{ev}^e(H_2O)$ in Figure 2 in order to provide a limit for the minimum value of the evaporation rate $J_{ev}(H_2O)$ at an ice film thickness $d_{He}$ of approximately 80 ± 10 nm as displayed in Figure 1B. We have observed in the past that $J_{ev}(H_2O)$ for a pure ice film of approximate thickness of 80 nm or less also slows down, presumably owing to island formation at the very end of pure thin ice film evaporation (Delval and Rossi, 2005). Therefore, results are becoming more difficult to interpret such that we halted the experiment at $t_{He}$. The ratio $r^{b/e} = J_{ev}^b(H_2O)/J_{ev}^e(H_2O)$ is displayed in Table 2 and is an operational

Deleted: quantitatively

evaporation range parameter that estimates the extent of decrease of $J_{ev}(H_2O)$ for a thick HCl-doped ice film of μm size down to thicknesses of approximately 80 nm.

At the start of the evaporation experiment the equilibrium vapor pressure of $H_2O$, $P_{eq}(H_2O)$, is that of pure ice (Delval et al., 2003; Delval and Rossi, 2004; Pratte et al., 2006) owing to the small values of $\chi_{HCl}^0$. Raoult's Law applies to such small values of $\chi_{HCl}$ but leads to unmeasurably small deviations from the observed vapor pressure of $H_2O$ which is that of pure ice. In fact, we have never observed an equilibrium vapor pressure that did not correspond to pure ice in the course of the present work that seems to be the consequence of the small average mole fractions of HCl in the $H_2O$/HCl system. This value of $P_{eq}(H_2O)$ is observed throughout the evaporation up to $t_{He}$ as the film is apparently sufficiently $H_2O$-rich to support an equilibrium vapour pressure characteristic of pure ice consistent with the published, albeit revised HCl/$H_2O$ phase diagram by Iannarelli and Rossi (2014). In view of the decreasing values of $J_{ev}(H_2O)$ displayed in Figure 2 the equilibrium vapour pressure of pure ice can only be maintained if the condensation rate coefficient $k_c$ for $H_2O$ adsorption decreases to the same extent as $J_{ev}(H_2O)$ in agreement with previous work (Delval et al., 2003; Delval and Rossi, 2004; Pratte et al., 2006) and the concept of microscopic reversibility.

Figure 1A displays both the QCMB signal (□) as well as the corresponding MS signal for evaporating $H_2O$ at m/e = 18 (◊). Akin to the $HNO_3/H_2O$ system studied previously (Delval and Rossi, 2005) we obtain a perfect match between the two signals for $t < t_D$ whereas for $t > t_D$ there is a significant discrepancy, especially at $t > 300$ s amounting to typically less than a factor of two. Such disagreement has been noted before for $HNO_3/H_2O$, albeit to a larger extent. The reason for this behaviour of the QCMB signal has not been studied in detail but may well stem from a structural rearrangement of the condensed phase during evaporation that will lead to a change in the calibration factor $C_f$ defined in Table 1 and in Delval and Rossi (2005). In view of the straightforward interpretation of the calibrated MS signal at m/e = 18 we have used it for the measurement of $J_{ev}(H_2O)$ at $t > t_D$ akin to the previous study on $HNO_3/H_2O$.

The accuracy with which both $t_{Hb}$ and $t_{He}$ can be determined depends on the temporal change of the background MS signal for HCl at m/e = 36 displayed in Figure 1B following the dosing of the thin ice film under stirred flow conditions. Figure 1B displays the MS signal at m/e = 36 as a function of time just before the start of HCl desorption at $t_{Hb}$ that is signalled by an increase in the MS intensity whereas $t_{He}$ corresponds to the return of the HCl signal to the decaying HCl background in comparison to a reference experiment in which the HCl

Deleted: a

Deleted: lie in

565 background was monitored as a function of time following the admission of the same HCl
566 dose in the absence of an ice film. We estimate that $t_{Hb}$ is determined to ± 10 s whereas $t_{He}$
567 may only be estimated to ± 100 s by virtue of the vanishing intensity of the HCl MS signal
568 compared to its slowly decaying background.
569 Previous work has established that the rate of deposition of HCl, $R_{HCl}$, in the range
570 $1x10^{13}$ to $5x10^{13}$ molecule $s^{-1}$ for the 0.78 $cm^2$ surface area of the Si-window leads to the
571 formation of a crystalline HCl hydrate, $HCl•xH_2O$, whereas values outside of this range
572 seemed to favor the formation of an amorphous $HCl/H_2O$ mixture (Delval et al., 2003). The
573 exact nature of this undoubtedly crystalline solid is still unknown. However, IR spectroscopic
574 work on hydroxonium salts of the type $H_3O^+X^-$ suggests that the $\nu_1$ and $\nu_3$ peak positions of
575 the symmetric and antisymmetric O-H stretch vibrations must correspond to a molecular
576 structure in which the distance between the cation and anion is unusually large (Desbat and
577 Huong, 1975; Iannarelli and Rossi, 2016). Recent work has shown that the presence of HCl
578 hexahydrate ($HCl•6H_2O$) under the present experimental conditions could be safely excluded,
579 however, the FTIR absorption spectrum clearly shows the presence of dissociated HCl within
580 the ice film (Iannarelli and Rossi, 2014). Akin to $HCl•6H_2O$ that is known to nucleate with
581 difficulty, crystallization of this unknown HCl hydrate seems to occur only under specific
582 conditions of temperature and/or HCl deposition. Owing to the quantitative control of HCl
583 deposition on the ice film in this work we infer the presence of at least two forms of HCl
584 hydrates in the temperature range chosen in analogy to previous work (Delval et al., 2003).
585 We clearly point out that the present work has been performed without simultaneous
586 spectroscopic control of the HCl/ice deposit that would have allowed the identification and/or
587 quantification of the molecular composition of the condensate. Because we lack a
588 spectroscopic probe for the ice film deposited on the QCMB in the present work we are
589 seeking a correlation between the type of $HCl/H_2O$ deposit, either crystalline or amorphous,
590 and the relevant HCl deposition parameters. Previous work has revealed a distinctly different
591 temporal dependence of $J_{ev}(H_2O)$ between the crystalline and amorphous HCl hydrates with
592 the extent of $H_2O$ evaporation from the film, both at low (Delval et al., 2003) and high
593 temporal resolution (Iannarelli and Rossi, 2014).
594 Datasets A and B have been characterized above in terms of a difference in the temporal
595 dependence of $J_{ev}(H_2O)$ as a function of increasing $\chi_{HCl}$ owing to $H_2O$ evaporation. Taking
596 one example of each set Figure 2 reveals a distinct difference between experiment 7 (set B)
597 and 11 (set A) performed at T = 195 and 192 K, respectively, despite comparable HCl
598 deposition parameters (Table 2). At $t > t_D$ $J_{ev}(H_2O)$ for experiment 7 decreases at once with

599 $\chi_{HCl}$ in contrast to experiment 11 whose $J_{ev}(H_2O)$ value gradually starts to decrease at roughly
600 the same value of $\chi_{HCl}$ as experiment 7. In addition, in both cases the extent of the decrease of
601 $J_{ev}(H_2O)$ is roughly equal between $t_D$ and $t_{Hb}$ within less than a factor of two. Set B data are in
602 marked contrast to set A independent of the magnitude of $\chi_{HCl}$ which is highlighted by a
603 comparison of experiment 11 (set A) and 4 (set B) at 192 and 190 K, respectively. The abrupt
604 decrease of $J_{ev}(H_2O)$ for set B as well as the gradual decline for set A both at $t_D$ occur before
605 HCl starts to evaporate from the sample at $t_{Hb}$ and appear therefore to be independent of $\chi_{HCl}$
606 within the range explored in the present work.
607 If we consider the mean value $<d_D>$ for data set B (Figures 4 and A2) we find 549.0 ±
608 120.0 nm compared to the 1'500 nm or so original ice thickness which corresponds to
609 approximately $8.5x10^{17}$ molecules of $H_2O$ spread out over 0.50 $cm^2$. These $H_2O$ molecules
610 are impacted by the presence of HCl to some extent because $J_{ev}(H_2O)$ is slowed down
611 significantly compared to pure ice. Previous results (Delval et al., 2003) on the deposition of
612 HCl on ice under conditions where the presence of an as yet unidentified crystalline hydrate
613 $HCl•xH_2O$ was confirmed by FTIR absorption led to the conclusion that on average the
614 amount of "trapped" $H_2O$ within $d_D$ corresponded to $1.2x10^{18}$ molecules starting with an
615 original 1 μm thick ice film that was subsequently doped with HCl. This quantity of $H_2O$,
616 when scaled from the 0.78 $cm^2$ area of the Si-window used for FTIR absorption to the area of
617 0.5 $cm^2$ of the QCMB leads to $7.7x10^{17}$ $H_2O$ that is in satisfactory agreement with the present
618 measurement of $d_D$ or $8.5x10^{17}$ $H_2O$ in the present work. We may add that the previous value
619 of $1.2x10^{18}$ $H_2O$ from the work of Delval et al. (2003) corresponding to $d_D$ obtained in that
620 work has been derived using HeNe interferometry which is a crude method for measuring the
621 film thickness.
622 Specifically, considering the low value of $d_D$ of experiments 1 and 10 (Table 2, Figure
623 4) we may define the behaviour of these condensates as "ice-like" because roughly 80% of the
624 ice sample of roughly 1.5 μm thickness has evaporated at $J_{ev}(H_2O)$ of pure $H_2O$ ice before it
625 slows down. This decrease of $J_{ev}(H_2O)$ is a kinetic effect and acts on both the rate of
626 evaporation as well as on the mass accommodation coefficient, the ratio of which remains
627 constant because the characteristic vapor pressure of pure ice is maintained until $t = t_{He}$ when
628 the sample runs out of $H_2O$ and HCl. For sample 1 this conclusion is not too surprising owing
629 to its extremely low HCl dose of 0.8 formal HCl monolayers. Sample 10 in comparison with
630 the other members of data set A allows us to conclude that $d_D$ is proportional to $T_{ice}$ for data
631 set A.

Low temperatures prevent rapid diffusion of HCl into the bulk of the ice film which leaves the majority of the total mass of the thin film deposited void of any HCl. Therefore, a large fraction of the total mass of the thin film deposit evaporates at values of $J_{ev}(H_2O)$ characteristic of pure ice before it decreases to lower values when the presence of HCl slows down $J_{ev}(H_2O)$. A quantitative, albeit simplified example may illustrate the situation in an approximate manner. Aguzzi et al. (2003) have measured the diffusion coefficient $D_{HCl}$ of HCl on single crystal (SC), condensed $H_2O$ vapour from the gas phase called C-ice and frozen liquid water ice (B for "bulk") at low temperatures. Taking the averaged value for B- and C-ice of $D_{HCl} = 2.3 \times 10^{-13}$ $cm^2$ $s^{-1}$ at 190 K we calculate the average distance taken for 3-D molecular diffusion of HCl in ice as 83 and 203 nm for a time horizon of 100 and 600 s, respectively (see time scale of Figure 1). This evaluation illustrates the point that during the time scale of the present experiments molecular diffusion of HCl encompasses the typical water ice interface that corresponds to a structurally perturbed region of the macroscopic thin ice films. Of course, HCl will diffuse to deeper layers into the bulk with increasing temperature taking into account the exponential dependence of D on temperature (Aguzzi et al., 2003). Although our experiment does not reveal the location of the thin layer of HCl-contaminated ice, plausibility suggests that it is located on top of the ice film at the gas-condensed interface. The corollary of this is that it is impossible to "cap" a pure ice sample with a thin layer of an atmospheric condensable gas of lower vapor pressure in the hope to lower the vapour pressure of the condensate or slow down $H_2O$ evaporation. This capping has been attempted many times, and examples abound. However, all attempts to lower the ice vapor pressure of the condensate using low amounts of polar contaminants of ice, such as $HNO_3$, HCl or HBr have proven futile to date (Biermann et al., 1998).

The other members of data set A are examples (experiments 2, 9, 11) with high values of $d_D$ at higher temperatures and higher HCl doses (Table 2). Because of higher presumed interfacial HCl concentrations these samples experience a decrease in $J_{ev}(H_2O)$ owing to rapid diffusion of HCl into ice that affects the kinetics of evaporation to some depths of the ice film corresponding to higher values of $d_D$. Both high HCl doses and high temperatures favor HCl contamination of deeper layers of the HCl film, hence high values of $d_D$.

Tentatively, we assign a crystalline, yet unknown molecular structure and stoichiometry to samples A in contrast to samples of dataset B that we identify with an amorphous structure in terms of a liquid $HCl/H_2O$ mixture of variable composition. The main argument in favour of this assignment comes from recent kinetic work performed by Iannarelli and Rossi (2016a) who show that both $J_{ev}(H_2O)$ as well as the corresponding mass accommodation coefficient or

Formatted: Subscript
Formatted: Subscript
Formatted: Superscript
Formatted: Superscript
Formatted: Superscript

the adsorption rate coefficient for $H_2O$ adsorption is highly scattered for crystalline HCl hexahydrate whereas the amorphous mixture shows a significantly smaller scatter of the experimental and thermodynamic values (Iannarelli and Rossi, 2014). Figure A3 and A4 in the Appendix show this substantial difference in experimental scatter for the amorphous $HCl/H_2O$ mixture (Figure A3) compared to crystalline HCl hexahydrate (Figure A4).

Figure 3 displays the range parameter $r^{b/e}$ as a function of $R_{HCl}$ for all data displayed in Table 2. It is noteworthy that $r^{b/e}$ is in the range 20 to 27 for set B experiments 3, 4, 7 and 8 compared to set A data that seem to be scattered throughout the range. Members of data set B show a common average range for both $d_D$ and $r^{b/e}$ which is the reason we tentatively assign these structures to amorphous liquid mixtures of high viscosity at the prevailing temperatures.

In conclusion, we take the simultaneous occurrence of the restricted range of the measured remaining thickness of ice $d_D$ = 549.0 ± 120.0 nm together with a similarly restricted range of $r^{b/e}$ between 20 and 27 as well as the substantial overlap in $R_{HCl}$ between the present and previous work (Delval et al., 2003) as an indication that set B evaporation experiments imply the presence of an amorphous $HCl/H_2O$ mixture. In contrast, the scatter of the set A data across the range of $r^{b/e}$ and $d_D$ values suggests the presence of an as yet unidentified crystalline HCl hydrate. If, and only if the HCl deposition conditions rapidly establish thermodynamic equilibrium, experiment 2 (low HCl flow rate) lies in the "ice" region in the temperature interval 192-210 K whereas experiment 11 (high HCl flow rate) should access crystalline HCl hexahydrate at 192 K but not at 210 K according to the revised $HCl/H_2O$ phase diagram of Iannarelli and Rossi (2014). It remains to be seen whether or not the published FTIR absorption spectrum in Delval et al (2003) turns out to be identical to the expected crystalline HCl hexahydrate invoked as condensate in set A molecules, similar HCl deposition parameters notwithstanding. This proposal awaits further confirmation from FTIR spectroscopic work that will be combined in the future with the QCMB measurement. At this point we reiterate our earlier statement that $T_{ice}$, $R_{HCl}$, $N^{dep}_{HCl}$ do apparently not control $J_{ev}(H_2O)$ of both datasets.

Deleted: .

## 5. ATMOSPHERIC IMPLICATIONS

The evaporation range parameter $r^{b/e}$ may be used to quantitatively evaluate the upper limit of the evaporative lifetime extension of thin ice films under conditions of $H_2O$ vapor subsaturation. In the interest of applying the data of the present work to atmospheric conditions we make the assumption that typical atmospheric Cirrus cloud particles of several

μm diameter may be approximated by macroscopic thin films used to obtain the present data. The time $t_{ev}$ in seconds to complete evaporation of an ice particle of radius r at a given relative humidity (rh) is given in equation 1 (Chiesa and Rossi, 2013; Iannarelli and Rossi, 2016a):

$$t_{ev} = \frac{(\frac{\rho N_L}{M})^{2/3}(\frac{r}{a})}{J_{ev}(1-rh)} \quad (1)$$

where $\rho$ is the density of ice (0.916 and 0.925 g $cm^{-3}$ at 273 and 173 K, respectively), M = 18 g $mol^{-1}$ for $H_2O$, r and a are the ice particle radius and the distance between two molecular layers in $H_2O$(ice), respectively (Iannarelli and Rossi, 2016a). Equation 1 is based on a simple layer-by-layer evaporation model of $H_2O$(ice) from a spherical ice particle following a zero-order rate law for $J_{ev}$ or a first order rate law for its inverse, namely $H_2O$ adsorption or condensation. For a 10 μm diameter ice particle approximated by thin film experiment 1 (Table 2) at rh = 80%, T = 192 K, $J_{ev} = 3x10^{16}$ molecule $s^{-1}$ $cm^{-2}$ (Petrenko and Whitworth, 1999) and $a = 4x10^{-8}$ cm we obtain $t_{ev}$ = 2050 s or 34 min. This is the value for a pure ice particle as $J_{ev}(H_2O)$ for pure ice has been used at the outset of the evaporation experiment and is a lower limit to the true evaporation time owing to the competition of mass transfer and heterogeneous chemistry (Seinfeld and Pandis, 1998). Using $r^{b/e}$ = 43 for experiment 1 $t_{ev}$ is calculated to be 15 minutes and 24 hours for a 100 nm and 10 μm diameter particle, respectively, whereas the evaporative lifetime of an analogous pure ice particle would be only 21 s for the 100 nm diameter pure ice particle. Cirrus ice particles are frequently in the lower tens of μm size range resulting in a longer evaporation time considering that the simple evaporation model scales linearly with the radius of the ice particle. In conclusion we may state that, owing to the lifetime extension of ice particles contaminated by HCl, $HNO_3$ or other volatile atmospheric trace gases such as HOCl, HOBr or HONO, small particles may have a chance to survive subsaturated regions of the atmosphere so as to function as cloud condensation or ice nuclei for the following cloud cycle (Delval and Rossi, 2004; 2005; Pratte et al., 2006).

We would like to stress, that the variable $r^{b/e}$ factor displayed in Table 2 leads to a significant increase in the evaporative lifetime of a contaminated ice particle and amounts to a **kinetic effect** that does not affect the equilibrium vapor pressure of the ice particle in question: it is that of pure ice from the start of the evaporation experiment to $t = t_{He}$ and therefore affects both the rate of evaporation and accommodation equally. However, in cases the sample has lost most of its mass the vapor pressure decreases and becomes somewhat uncertain. In the present case the above statement is correct for $t = t_{Hb}$, that is before halogen

evaporation. Of note is the fact, that the accommodation coefficient $\alpha$ is frequently less than unity, in contrast to what is often assumed, which will lower the rate of evaporation for pure ice, hence increase the evaporative lifetime of pure ice particles for $T \geq 180$ K as proposed in previous work (Delval and Rossi, 2004; 2005; Pratte et al., 2006).

As a token example of potential atmospheric importance of the measured evaporative lifetimes of ice particles laced with condensable atmospheric trace gases we may take the formation, persistence and evaporation of contrails and Cirrus clouds in the UT/LS. These are ice clouds forming on non-volatile ice nuclei at the corresponding temperature and relative humidity conditions and also frequently serve as reaction sites for heterogeneous atmospheric reactions in connection with ozone depletion and chlorine activation chemistry in the LS. Under certain conditions, Schumann and coworkers used the concept of the increase of the evaporative lifetimes of contaminated ice particles in aviation contrails occurring mostly in the UT, but sometimes also in the LS, in order to explain the persistence of ice clouds below ice saturation conditions up to a certain time duration. Ice clouds have a significant radiative forcing effect that is of interest in evaluating the climate forcing of high-flying aircraft in future aviation scenarios (Lewellen, 2014; Schumann et al, 2017; 2017a). However, the results of the present work show that the rate of evaporation of ice films doped with small amounts of acidic trace gases significantly slows down in a complex manner over the evaporation history of the film or particle, and that the application of equation (1) to atmospheric situations should be carried out with caution.

## CONCLUSIONS

Despite the scatter of the values of $r^{b/e}$ and $d_D$ in dataset A displayed in Figures 3 and 4 and the apparent lack of influence of the deposition parameters ($T_{ice}$, $R_{HCl}$, $N^{dep}_{HCl}$) on $J_{ev}(H_2O)$ we may state several key points from the present work:

(a) We observe two types of behaviour, both complex, as far as the temporal change of $J_{ev}(H_2O)$ with on-going evaporation of $H_2O$ from a $HCl/H_2O$ condensate is concerned. We have named it sets A and B that represent limiting behaviour as not all performed experiments fit into this scheme.

(b) At low temperature or low dose of deposited HCl ($N^{dep}_{HCl}$) set A samples, especially samples 1 and 10, reveal an “ice-like” behaviour that corresponds to a low value of $d_D$. This means that the $HCl/H_2O$ condensate evaporates a large fraction of the sample thickness at a value of $J_{ev}(H_2O)$ characteristic of pure ice before slowing

down at increasing mole fraction of HCl upon $H_2O$ evaporation. This corresponds to a two-phase system consisting of a major ice-like and a minor HCl/$H_2O$ phase having both significantly different values of $J_{ev}(H_2O)$.

(c) High values of $d_D$ are observed at high $T_{ice}$ or $N^{dep}_{HCl}$ values for set A samples. This means that the sample evaporates $H_2O$ at $J_{ev}(H_2O)$ characteristic of pure ice for a relatively short time of its evaporation history because the quantity of HCl is sufficient to decrease $J_{ev}(H_2O)$ already at high values of $d_D$ by rapidly diffusing to deeper layers of the ice film. An equivalent way of expressing the point would be to state that $d_D$ which is an indicator of the total mass of the ice film, is proportional to $T_{ice}$ for Set A.

(d) Set A samples generally show scattered values of both $d_D$ and $r^{b/e}$ values that we attribute to the existence of a two-phase binary system, namely a pure ice and a crystalline HCl hydrate phase of as yet unknown stoichiometry HCl•x$H_2O$, but probably HCl Hexahydrate, at least for temperatures lower than 192 K. At first the pure ice phase starts to evaporate as a whole for a fairly long time at characteristic values of $J_{ev}(H_2O)$ until the pure ice phase has disappeared, followed by the crystalline HCl/$H_2O$ phase at a lower rate of $J_{ev}(H_2O)$ to attain the characteristic value for the evaporation of the crystalline HCl•x$H_2O$ phase.

(e) Set B samples are tentatively identified as single phase binary amorphous mixtures of HCl/$H_2O$ whose kinetic properties are uniform, thus fairly independent of the HCl concentration at the gas-condensed phase interface. The observation of a medium size average value for both $r^{b/e}$ and $d_D$ is consistent with these observations and manifests itself as a continuous, yet gradual decrease of $J_{ev}(H_2O)$ with increasing $\chi_{HCl}$. It is in distinct contrast to Set A where $J_{ev}(H_2O)$ values are those of pure ice until the ice phase has completely evaporated followed by a gradual decline of $J_{ev}(H_2O)$ when the crystalline HCl hydrate starts to decompose.

(f) It must be recalled that the vapour pressure of $H_2O$ remained that of pure ice during most of the thickness of the $H_2O$/HCl condensate down to approximately 80 nm at which point we halted the evaporation experiment. This result is expected based on Raoult's law owing to the small average HCl mole fractions in doped ice used in the present work: It would make the decrease of the $H_2O$ saturation vapour pressure unmeasurably small. The present results therefore primarily address the **kinetics** of $H_2O$ evaporation which changes with the total mass of the thin film condensate and the concomitant increase in HCl concentration and/or mole fraction.

301

Deleted: ¶

## References


Abbatt, J. P. D. Interactions of atmospheric trace gases with ice surfaces: Adsorption and reactions, Chem. Rev. **2003**, *103*, 4783-4800.

Aguzzi, A.; Flückiger, B.; Rossi, M.J. The nature of the interface and the diffusion coefficient of HCl/ice and HBr/ice in the temperature range 190–205 K, Physical Chemistry Chemical Physics **2003**, *5*, 4157-4169.

Banham, S. F.; Horn, A. B.; Koch, T. G.; Sodeau, J. R. Ionisation and solvation of stratospherically relevant molecules on ice films, Faraday Discuss. **1995**, *100*, 321-332.

Biermann, U.; Crowley, J. N.; Huthwelker, T.; Moortgat, G. K.; Crutzen, P. J.; Peter, T. FTIR studies on lifetime prolongation of stratospheric ice particles due to NAT coating, Geophys. Res. Lett. **1998**, *25*, 3939-3942.

Bolton, K.; Petterson, J. B. C. Ice-Catalyzed Ionization of Hydrochloric Acid, J. Amer. Chem. Soc. **2001**, *123*, 7360-7363.

Borrmann, S.; Solomon, S.; Dye, J.E.; Luo, B. The potential of cirrus clouds for heterogeneous chlorine activation, Geophys. Res. Lett. **1996**, *23*, 2133-2136.

Bournel, F.; Mangeney, C.; Tronc, M.; Laffon, C.; Parent, P. Acidity of hydrogen chloride at the surface of low-temperature 40–150 K water-ice films, Phys. Rev. B **2002**, *65*, 201404-1 to 201404-4.

Buch, V.; Dubrovskij, A., Mohamed, F.; Parinello, M.; J. Sadlej, J.; Hammerich, A.D.; Devlin, J.P. Protonated Water HCl Hydrates as Model Systems for Protonated Water, J. Phys. Chem. A 112, 2144-2161, 2008.

Buch, V.; Sadlej, J.; Aytemiz-Uras, N.; Devlin, J. P. Ice-Catalyzed Ionization of Hydrochloric Acid J. Phys. Chem. A **2002**, *106*, 9374-9389.

Chiesa, S.; Rossi, M. J. HCl•6$H_2O$ is metastable - IR spectroscopy, phase transitions and kinetic/thermodynamic properties in the range 170-200 K, Atm. Chem. Phys. **2013**, *13*, 11905-11923.

Chu, L. T.; Leu, M.-T.; Keyser, L. F. Uptake of HCI in Water Ice and Nitric Acid Ice Films, J. Phys. Chem. **1993**, *97*, 7779-7785.

Delval, C.; Flückiger, B., Rossi, M. J. The Rate of Water Vapor Evaporation from Ice Substrates in the presence of HCl and HBr: Implications for the Lifetime of atmospheric Ice Particles, Atmos. Chem. Phys. **2003**, *3*, 1131-1145.


**Formatted:** Font: (Default) Times New Roman, 12 pt, English (United States)

**Formatted:** Font: (Default) Times New Roman, 12 pt, English (United States)

**Formatted:** English (United States)

**Formatted:** Font: (Default) Times New Roman, 12 pt, English (United States)

**Formatted:** Left, Don't adjust space between Latin and Asian text, Don't adjust space between Asian text and numbers

**Formatted:** English (United States)

**Formatted:** Font: (Default) Times New Roman, 12 pt, English (United States)

**Formatted:** Font: (Default) Times New Roman, 12 pt

**Formatted:** Font: (Default) Times New Roman, 12 pt, English (United States)

**Formatted:** Font: Bold

**Formatted:** Font: Italic

**Formatted:** Left, Indent: Left: 0 cm, Hanging: 1 cm, Don't adjust space between Latin and Asian text, Don't adjust space between Asian text and numbers

**Formatted:** Font: (Default) Times New Roman, 12 pt, Not Bold, English (United States)

**Formatted:** Font: (Default) Times New Roman, 12 pt, Not Bold

**Formatted:** Font: (Default) Times New Roman, 12 pt, Not Bold, English (United States)

**Formatted:** Font: Bold

**Formatted:** Font: Italic

836 Delval, C.; Rossi, M. J. The kinetics of condensation and evaporation of $H_2O$ from pure ice in
837 the range 173 to 223 K: A quartz crystal microbalance study, Phys. Chem. Chem.
838 Phys. **2004**, *6*, 4665-4676.
839 Delval, C.; Rossi, M. J. The influence of monolayer amounts of $HNO_3$ on the evaporation rate
840 of $H_2O$ over ice at $179 \leq T/K \leq 208$: A quartz crystal microbalance study, J. Phys.
841 Chem. A **2005**, *109*, 7151-7165.
842 Delzeit, L.; Rowland, B.; Devlin, J. P. Infrared Spectra of HCl Complexed/Ionized in
843 Amorphous Hydrates and at Ice Surfaces in the 15-90 K Range, J. Phys. Chem. **1993**,
844 *97*, 10312-10318.
845 Delzeit, L.; Rowland, B.; Devlin, J. P. Ice Surface Reactions with Acids and Bases, J. Phys.
846 Chem. **1993a**, *97*, 10312-10318.
847 Delzeit, L.; Powell, K.; Uras, N.; Devlin, J. P. Ice Surface Reactions with Acids and Bases, J.
848 Phys. Chem. B **1997**, *101*, 2327-2332.
849 Desbat, B.; Huong, P. V. Spectres i.r. et Raman des sels d'hydroxonium $H_3O^+Cl^-$, $H_3O^+Br^-$ et
850 $H_3O^+SbCl_6^-$, Spectrochim. Acta, Part A **1975**, *31*, 1109-1114.
851 Devlin, J. P.; Uras, N.; Sadlej, J.; Buch, V. Discrete stages in the solvation and ionization of
852 hydrogen chloride adsorbed on ice particles, Nature **2002**, *414*, 269-271.
853 Devlin, J.P.; Kang, H. Comment on «HCl adsorption on ice at low temperature: a combined
854 X-ray absorption, photoemission and infrared study» by P. Parent, J. Lasne, G.
855 Marcotte and C. Laffon, Phys. Chem. Chem. Phys. **2011**, 13, 7142, Phys. Chem.
856 Chem. Phys. **2012**, *14*, 1048-1049.
857 Donsig, H. A.; Vickerman, J. C. Dynamic and static secondary ion mass spectrometry studies
858 of the solvation of HCl by ice, J. Chem. Soc. Faraday Trans. **1997**, *93*, 2755-2761.
859 Ferriso, C. G.; Hornig, D. F. Infrared Spectra of Oxonium Halides and the Structure of the
860 Oxonium Ion, J. Chem. Phys. **1955**, *23*, 1464-1468.
861 Flückiger, B.; Thielmann, A.; Gutzwiller, L.; Rossi, M. J. Real-Time Kinetics and
862 Thermochemistry of the Uptake of HCl, HBr and HI on Water Ice in the Temperature
863 Range 190 to 210 K, Ber. Bunsenges. Phys. Chem. **1998**, *102*, 915-928.
864 Flückiger, B.; Delval, C. Unpublished observations on the behavior of dangling hydrogen
865 bonds (dH) in the presence of HCl at T < 120 K (2002). In essence, the dH absorption
866 intensity at 3396 $cm^{-1}$ did not decrease in the presence of small HCl partial pressures
867 on the order of 3 x $10^{-6}$ Torr at ambient temperature or 4 ppb (Fig. 2.16, Christophe
868 Delval, PhD Thesis no. 3159, EPFL (2005))

Deleted: ,

Flückiger, B.; Rossi, M. J. Common Precursor-mediated Reaction Mechanism for the Heterogeneous Interaction of $D_2O$, HCl, HBr and HOBr on Ice at low Temperatures, J. Phys. Chem. A **2003**, *107*, 4103-4115.

Gertner, B. J.; Hynes, J. T. Molecular Dynamics Simulation of Hydrochloric Acid Ionization at the Surface of Stratospheric Ice, Science **1996**, *271*, 1563-1566.

Gilbert, A. S.; Sheppard, N. Infra-red Spectra of the Hydrates of Hydrogen Chloride and Hydrogen Bromide Absorption Bands of the $H_5O_2^+$ Species, J. Chem. Soc. Faraday Trans. **1973**, *69*, 1628-1642.

Graedel, T. E.; Keene, W. C. Tropospheric budget of reactive chlorine, Global Biogeochemical Cycles **1995**, *9*, 47-77.

Graham, J. D.; Roberts, J. T. Interaction of HCl with crystalline and amorphous ice: implications for the mechanisms of ice-catalyzed reactions, Geophys. Res. Lett. **1995**, *22*, 251-254.

Graham, J. D.; Roberts, J. T. Formation of HCl•$6H_2O$ from ice and HCl under ultrahigh vacuum, Chemom. Intell. Lab. Systems **1997**, *37*, 139-148.

Hanson, D.R. ; Ravishankara, A.R. Investigation of the Reactive and Nonreactive Processes Involving $ClONO_2$ and HCl on Water and Nitric Acid Doped Ice, J. Phys. Chem. **1992**, *96*, 2682-2691.

Houghton, J. T. et al.; eds., *Climate Change 2001: The Scientific Basis* (Cambridge Univ. Press, New York 2001).

Hynes, R. G.; Mössinger, J.; Cox, R. A. The interaction of HCl with water-ice at tropospheric temperatures, Geophys. Res. Lett. **2001**, *28*, 2827-2830.

Iannarelli, R.; Rossi, M. J. $H_2O$ and HCl trace gas kinetics on crystalline and amorphous HCl hydrates in the range 170 to 205 K: The HCl/$H_2O$ Phase Diagram revisited, Atm. Chem. Phys. **2014**, *14*, 5183-5202.

Iannarelli, R.; Rossi, M. J. The mid-IR absorption cross sections of α- and β-NAT ($HNO_3$●$3H_2O$) in the range 170 to 185 K and of metastable NAD ($HNO_3$●$2H_2O$) in the range 172-182 K, J. Geophys. Res. Atmos. **2016**, *120*, 11707-11727.

Iannarelli, R.; Rossi, M. J. Heterogeneous Kinetics of $H_2O$, $HNO_3$ and HCl on $HNO_3$ hydrates (α-NAT, β-NAT, NAD) in the range 175-200 K, Atm. Chem. Phys. **2016a** *16*, 11937-11960.

Jensen, E. J.; Toon, O. B.; Vay, S. A.; Ovarlez, J.; May, R.; Bui; T. P.; Twohy, C. H.; Gandrud, B. W.; Pueschel, R. F., Schumann, U. Prevalence of ice-supersaturated

regions in the upper troposphere: Implications for optically thin ice cloud formation, J. Geophys. Res. **2001**, *106*, 17253-17266.

Kang, H.; Shin, T. H.; Park, S. P.; Kim, I. K.; Han, S. J. Acidity of Hydrogen Chloride on Ice J. Am. Chem. Soc. **2000**, *122*, 9842-9843.

Kong, X.; Waldner, A.; Orlando, F.; Artiglia, L.; Huthwelker, Th.; Ammann, M.; Bartels-Rausch, Th. Coexistence of Physisorbed and Solvated HCl At Warm Ice Surfaces, J. Phys. Chem. Lett. **2017**, *8*, 4757-4762.

Kuhs, W.F.; Sippel, C.; Falenty, F.; Hansen, C.T. Extent and relevance of stacking disorder in "ice $I_c$", PNAS (Proceedings of the National Academy of Science (USA)), **2012**, 109, 21259- 21264.

Leu, M.-T. ; Moore, S.B.; Keyser, L.F. Heterogeneous Reactions of Chlorine Nitrate and Hydrogen Chloride on Type I Polar Stratospheric Clouds J. Phys. Chem. **1991**, *95*, 7763-7771.

Lewellen, D.C. Persistent Contrails and Contrail Cirrus. Part II: Full Lifetime Behavior, J. Atmos. Sci. **2014**, *71*, 4420-4438.

Lu, Q. B. ; Sanche, L. Large enhancement in dissociative electron attachment to HCl adsorbed on ice via transfer of presolvated electrons J. Chem. Phys. **2001**, *115*, 5711-5713.

Lundgren, J. O.; Olovson, I. Hydrogen Bond Studies. XV. The Crystal Structure of Hydrogen Chloride Dihydrate, Acta Cryst. **1967**, *23*, 966-970.

Lundgren, J. O.; Olovson, I. Hydrogen Bond Studies. XVI. The Crystal Structure of Hydrogen Chloride Trihydrate, Acta Cryst. **1967a**, *23*, 971-976.

Marcy, T. P; Fahey, D. W.; Gao, R. S.; Popp, P. J.; Richard, E. C.; Thompson, T. L.; Rosenlof, K. H.; Ray, E. A.; Salawitch, R. J.; Atherton, C. S.; Bergmann, D. J.; Ridley, B. A.; Weinheimer, A. J.; Loewenstein, M.; Weinstock, E. M.; Mahoney, M. J. Quantifying Stratospheric Ozone in the Upper Troposphere with *in situ* Measurements of HCl, Science **2004**, *304*, 261-265.

Marti, J.; Mauersberger, K. A survey and new measurements of ice vapor pressure at temperatures between 170 and 250 K, Geophys. Res. Lett. **1993**, *20*, 363-366.

Mauersberger, K.; Krankowsky, D. Vapor pressure above ice at temperatures below 170 K, Geophys. Res. Lett. **2003**, *30*, 1121-1124.

Oppliger, R.; Allanic, A.; Rossi, M. J. Real-Time Kinetics of the Uptake of HOBr and $BrONO_2$ on Ice and in the Presence of HCl in the Temperature Range 190 – 200 K, J. Phys. Chem. A **1997**, *101*, 1903-1911.

Deleted: ,
Deleted: ,
Deleted: ,
Deleted: ,
Deleted: ,
Deleted: ,
Deleted: ,
Deleted: ,
Deleted: ,
Deleted: ,
Deleted: ,
Deleted: ,

950 Ortega, I. K.; Escribano, R.; Fernandez-Torre, D.; Herrero, V. J.; Maté, B.; Moreno, M. A.
951 The HCl hexahydrate: RAIR spectra and theoretical investigation, Chem. Phys. Lett.
952 **2004**, *396*, 335-340.
953 Parent, P.; Laffon, C. Adsorption of HCl on the Water Ice Surface Studied by X-ray
954 Absorption Spectroscopy, J. Phys. Chem. B **2005**, *109*, 1547-1553.
955 Parent, P.; Lasne, J.; Marcotte, G.; Laffon, C. HCl adsorption on ice at low temperature: a
956 combined X-ray absorption, photoemission and infrared study, Phys. Chem. Chem.
957 Phys. **2011**, *13*, 7142-7148.
958 Parent, P.; Lasne, J.; Marcotte, G.; Laffon, C. Reply to the "Comment on "HCl adsorption on
959 ice at low temperature: a combined X-ray absorption, photoemission and infrared
960 study"" by J.P. Devlin and H. Kang, Phys. Chem. Chem. Phys. 2012, 14,
961 DOI:10.1039/c1cp22007a, Phys. Chem. Chem. Phys. **2012**, *14*, 1050-1053.
962 Petrenko, V. F.; Whitworth, R. W. *The Physics of Ice*, Oxford University Press, **1999**.
963 Pratte, P.; van den Bergh, H.; Rossi, M. J. The kinetics of $H_2O$ vapor condensation and
964 evaporation on different types of ice in the range 130-210 K, J. Phys. Chem. A **2006**,
965 *110*, 3042-3058.
966 Schriver-Mazzuoli, L.; Schriver A.; Hallou, A. IR-reflection-absorption spectra of thin water
967 ice films between 10 and 160 K at low pressure, J. Mol. Struct. **2000**, 554, 289-300.
968 Schumann, U.; Baumann, R.; Baumgardner, D.; Bedka, S.T.; Duda, D.P.; Freudenthaler, V.;
969 Gayet, J.-F.; Heymsfield, A.J.; Minnis, P.; Quante, M.; Raschke, E.; Schlager, H.;
970 Vazquez-Navarro, M.; Voigt, C.; Wang, Z. Properties of individual contrails: A
971 compilation of observations and some comparisons, Atm. Chem. Phys. **2017**, *17*, 403-
972 438.
973 Schumann, U.; Kiemle, C.; Schlager, H.; Weigel, R.; Borrmann, S.; D'Amato, F.; Krämer,
974 M.; Matthey, R.; Protat, A.; Voigt, C.; Volk, M. Long-lived contrails and convective
975 cirrus above the tropical tropopause, Atm. Chem. Phys. **2017a**, *17*, 2311-2346.
976 Seinfeld, J. H.; Pandis, S. N. *Atmospheric Chemistry and Physics, from Air Pollution to*
977 *Climate Change*, John Wiley and Sons, Inc. (**1998**).
978 Solomon, S.; Garcia, R. R.; Rowland, F. S.; Wuebbles, D. J. On the Depletion of Antarctic
979 Ozone, Nature **1986**, *321*, 755-758.
980 Solomon, S.; Borrmann, S.; Garcia, R. R.; Portmann, R.; Thomason, L.; Poole, L. R.; Winker,
981 D.; McCormick, M. P. Heterogeneous chlorine chemistry in the tropopause region, J.
982 Geophys. Res. (Atmos) **1997**, *102*, 21411-21429.

Deleted: ,
Deleted: ,
Deleted: ,
Deleted: ,
Deleted: ,
Deleted: ,
Deleted: ,
Deleted: ,
Deleted: ,

Taesler, I.; Lundgren, J. O. Hydrogen Bond Studies. CXXIX. An X-Ray Determination of the Crystal Structure of Hydrogen Chloride Hexahydrate, $H_9O_4^+Cl^-•2H_2O$, Acta Crystallogr. B **1978**, *34*, 2424-2428.

Tolbert, M. A.; Rossi, M. J.; Malhotra, R.; Golden, D. M. Reaction of Chlorine Nitrate with Hydrogen Chloride and Water at Antarctic Stratospheric Temperatures, Science **1987**, *238*, 1258-1260.

Uras, N.; Rahman, M.; Devlin, J. P. Covalent HCl at the Surface of Crystalline Ice at 125 K: The Stable Phase at Submonolayer Levels J. Phys. Chem. B **1998**, *102*, 9375-9377.

WMO (World Meteorological Organization) *Scientific Assessment of Ozone Depletion 2002*, Global Ozone Research and Monitoring Project, report no. 47, Geneva, **2003**.

Xueref, I.; Dominé, F. FTIR spectroscopic studies of the simultaneous condensation of HCl and $H_2O$ at 190K – Atmospheric applications Atmos. Chem. Phys. **2003**, *3*, 1779-1789.

Yoon, Y. K.; Carpenter, G. B. The Crystal Structure of Hydrogen Chloride Monohydrate, Acta Cryst. **1959**, *12*, 17-20.

Zerefos, C. S.; Eleftheratos, K.; Balis, D. S.; Zanis, P.; Tselioudis, G.; Meleti, C. Evidence of impact of aviation on Cirrus cloud formation, Atmos. Chem. Phys. **2003**, *3*, 1633-1644.

The authors declare no competing interests regarding the present work.

**Acknowledgement**

We sincerely thank Dr. R. Iannarelli for Figures A3 and A4 displayed in the Appendix. We also would like to thank the Swiss National Science Foundation (SNSF) for unfailing support over the years. This work has been performed under SNSF grants no. 20-65299.01 and 200020-105471.

Table 1: Hardware parameters of both cryogenic sample supports

| | Si Optical Window | QCM | |
|---|---|---|---|
| Reactor temperature $T_r$ [K] | 320 | | |
| Reactor volume $V_r$ [$cm^{-3}$] | 2350 | | |
| Conversion factor (1/RT) Conv [molec $cm^{-3}$ $Torr^{-1}$] with R=62398 [Torr $cm^3$ $mol^{-1}$ $K^{-1}$] | $3.0 \cdot 10^{16}$ (1) | | |
| Sample surface area [$cm^2$] | 0.78 | 0.50 | |
| $H_2O$ collision frequency with ice sample $\omega_{H2O}$ [$s^{-1}$] | 5.08 | 3.26 | |
| $H_2O$ effusion rate constant of calibrated leak $k_{esc}(H_2O)$ [$s^{-1}$] | 0.064 | | |
| MS calibration factor for $H_2O$ (m/z=18, Stirred Flow) $C_{18}^{S-Flow}$ [molec $s^{-1}$ $A^{-1}$] | $2.4 \cdot 10^{24}$ | | |
| MS calibration factor for $H_2O$ (m/z=18, Dynamic ) $C_{18}^{dyn}$ [molec $s^{-1}$ $A^{-1}$] | $1.7 \cdot 10^{25}$ | | |
| HCl collision frequency with ice sample $\omega_{HCl}$ [$s^{-1}$] | 3.59 | 2.31 | |
| HCl effusion rate constant of calibrated leak $k_{esc}$(HCl) [$s^{-1}$] | 0.047 | | |
| MS calibration factor for HC1 (m/z=36, Stirred Flow) $C_{36}^{S-Flow}$ [molec $s^{-1}$ $A^{-1}$] | $3.9 \cdot 10^{24}$ | | |
| MS calibration factor for HC1 (m/z=36, Dynamic) $C_{36}^{dyn}$ [molec $s^{-1}$ $A^{-1}$] | $6.3 \cdot 10^{24}$ | | |
| Calculated escape orifice area $A_{esc}$ [$mm^2$] | 1.0 | | |
| | d = $10^4$ Å or 1.0 µm for O.D.= 1.08 [A](2) at 3260 $cm^{-1}$ | Calibration Factor | |
| | | Temperature [K] | ratio(3) |
| | | 170 | 9.0 |
| | | 180 | 8.0 |
| | | **190** | **7.8** |
| | | 193 | 6.0 |
| | | 205 | 2.0 |
| | | 208 | 1.9 |

[1] Wall temperature of the reactor at T = 320 K

[2] See (Delval et al., 2003)

[3] Corresponds to the ratio between the true number of molecules present on the QCM support and the number of molecules displayed by the IC5 controller (Delval et al., 2004)

**Table 2 : Representative experimental results for the kinetics of $H_2O$ evaporation in the presence of HCl for increasing HCl deposition temperatures at given rates of deposition $R_{HCl}$ and doses of HCl $N_{HCl}^{dep}$. In the first column the number refers to the corresponding experiment and identifies the data displayed in Figure 2**

| Experiment number | $T_{ice}$ | $d_0$ | $N^0_{H2O}$ | $R_{HCl}$ | $t_{dep}$ | $N^{dep}_{HCl}$ | HCl | $N^{evap}_{HCl}$ | $\chi^0_{HCl}$ | $d_D$ | $J^b_{ev}$ | $J^e_{ev}$ | $r^{b/e}$ |
|---|---|---|---|---|---|---|---|---|---|---|---|---|---|
| | [K] | [Å] | [molec] | [molec $s^{-1}$] | [s] | [molec] | ML | [molec] | | [Å] | [molec $cm^{-2}$ $s^{-1}$] | [molec $cm^{-2}$ $s^{-1}$] | |
| **10** | 174 | 15230 | $2.4\cdot10^{18}$ | $6.4\cdot10^{12}$ | 94 | $6.0\cdot10^{14}$ | 4.8 | $4.7\cdot10^{14}$ | $2.5\cdot10^{-4}$ | 2733 | $1.9\cdot10^{15}$ | $4.4\cdot10^{14}$ | 4.3 |
| **5** | 188 | 13318 | $2.0\cdot10^{18}$ | $1.3\cdot10^{13}$ | 66 | $8.7\cdot10^{14}$ | 7.0 | $8.9\cdot10^{14}$ | $4.4\cdot10^{-4}$ | 4540 | $1.2\cdot10^{16}$ | $3.9\cdot10^{15}$ | 3.1 |
| **4** | 190 | 14016 | $2.1\cdot10^{18}$ | $4.2\cdot10^{13}$ | 126 | $5.4\cdot10^{15}$ | 43.2 | $3.6\cdot10^{15}$ | $2.6\cdot10^{-3}$ | 6360 | $2.9\cdot10^{16}$ | $1.4\cdot10^{15}$ | 20.7 |
| **6** | 190 | 13886 | $2.1\cdot10^{18}$ | $3.9\cdot10^{13}$ | 56 | $2.2\cdot10^{15}$ | 17.6 | $1.8\cdot10^{15}$ | $1.0\cdot10^{-3}$ | 12861 | $3.4\cdot10^{16}$ | $1.7\cdot10^{16}$ | 2.0 |
| **1** | 192 | 14926 | $2.3\cdot10^{18}$ | $3.1\cdot10^{12}$ | 36 | $1.0\cdot10^{14}$ | 0.8 | $1.8\cdot10^{14}$ | $4.3\cdot10^{-5}$ | 2823 | $2.9\cdot10^{16}$ | $7.1\cdot10^{14}$ | 40.8 |
| **2** | 192 | 14682 | $2.3\cdot10^{18}$ | $8.0\cdot10^{11}$ | 356 | $2.6\cdot10^{14}$ | 2.1 | $1.6\cdot10^{14}$ | $1.1\cdot10^{-4}$ | 6817 | $3.2\cdot10^{16}$ | $6.5\cdot10^{14}$ | 49.2 |
| **11** | 192 | 14420 | $2.2\cdot10^{18}$ | $5.4\cdot10^{12}$ | 108 | $5.4\cdot10^{14}$ | 4.3 | $6.8\cdot10^{14}$ | $2.4\cdot10^{-4}$ | 7717 | $4.0\cdot10^{16}$ | $7.9\cdot10^{14}$ | 50.6 |
| **3** | 193 | 14423 | $2.2\cdot10^{18}$ | $3.5\cdot10^{12}$ | 220 | $7.0\cdot10^{14}$ | 5.6 | $8.1\cdot10^{14}$ | $3.2\cdot10^{-4}$ | 5659 | $4.9\cdot10^{16}$ | $1.8\cdot10^{15}$ | 27.2 |
| **7** | 195 | 12614 | $1.9\cdot10^{18}$ | $4.3\cdot10^{12}$ | 45 | $1.9\cdot10^{14}$ | 1.5 | $1.8\cdot10^{14}$ | $1.0\cdot10^{-4}$ | 5325 | $4.6\cdot10^{16}$ | $2.0\cdot10^{15}$ | 23.0 |
| **8** | 205 | 13505 | $2.1\cdot10^{18}$ | $1.6\cdot10^{13}$ | 36 | $5.9\cdot10^{14}$ | 4.7 | $3.0\cdot10^{14}$ | $2.8\cdot10^{-4}$ | 4607 | $2.0\cdot10^{17}$ | $1.0\cdot10^{16}$ | 20.0 |
| **9** | 210 | 13134 | $2.0\cdot10^{18}$ | $3.5\cdot10^{12}$ | 84 | $3.0\cdot10^{14}$ | 2.4 | $1.9\cdot10^{14}$ | $1.5\cdot10^{-4}$ | 12136 | $3.0\cdot10^{17}$ | $1.8\cdot10^{16}$ | 16.7 |

**Figure Captions**

Figure 1: Typical experimental protocol of the evaporation at 192 K of an approximately 1.2 μm thick ice film doped with $5.4 \cdot 10^{14}$ molecules of HCl. This illustration corresponds to experiment 11 of Table 2. (○): ice thickness monitored by QCM (Å), (□): "apparent" $H_2O$ evaporative flux, $J^{QCM}_{ev}$ , monitored by QCM (molecule $cm^{-2}$ $s^{-1}$), (+): $I^{18}$ MS signal for $H_2O$, (×): $I^{36}$ MS signal for HCl (A), (◊): $J^{18}_{ev}$ evaporative flux calculated from $I^{18}$ (molecule $cm^{-2}$ $s^{-1}$), (Δ): Int($J^{18}_{ev}$) time integral of $J^{18}_{ev}$ (molecule $cm^{-2}$).

Figure 2: Change of the evaporative flux $J_{ev}(H_2O)$ as a function of the HCl mole fraction ($\chi_{HCl}$) for the cases presented in Table 2 color-coded according to the corresponding experiment number in Table 2. The colored and circled numbers on axis "b" (left) correspond to $J_{ev}(H_2O)$ of pure ice before HCl deposition, the ones on axis "e" (right) are $J_{ev}(H_2O)$ at t = $t_{He}$ at the end of HCl evaporation. The colored circles in the data field mark the value of $J_{ev}(H_2O)$ after HCl deposition at t = $t_0$ and are equal to $J_{ev}(H_2O)$ of pure ice. The start of any particular $J_{ev}(H_2O)$ curve as a continuous solid (bold) line occurs at t = $t_D$ at 85% of $J_{ev}(H_2O)$ at t = 0 (pure ice value, colored circle or circled number on axis "b" to the left) and ends at $t_{Hb}$, the beginning of HCl evaporation as displayed in Figure 1B.

Figure 3: Synopsis of the dependence of the evaporation range parameter $r^{b/e}$ on the rate of deposition $R_{HCl}$ of HCl for temperatures between 188 and 210 K. Each point is marked with the total number of HCl molecules ($N_{HCl}$) deposited on the ice film , the temperature of the ice film at HCl deposition and the experiment number (bold) referring to Table 2. The hashed area encompasses $r^{b/e}$ values for dataset B (experiments 3,4,7,8). The color code goes from low (blue) over medium (green) to high (red) temperatures.

Figure 4: Synopsis of the dependence of $d_D$ on the rate of deposition $R_{HCl}$ of HCl for temperatures between 188 and 210 K. Each point is marked with the total number of HCl molecules ($N_{HCl}$) deposited on the ice film, the temperature of the ice film at HCl deposition and the experiment number (bold font) referring to Table 2. The hashed area encompasses $d_D$ values for dataset B (experiments 3,4,7,8). The color code goes from low (blue) over medium (green) to high (red) temperatures.

Figure 1

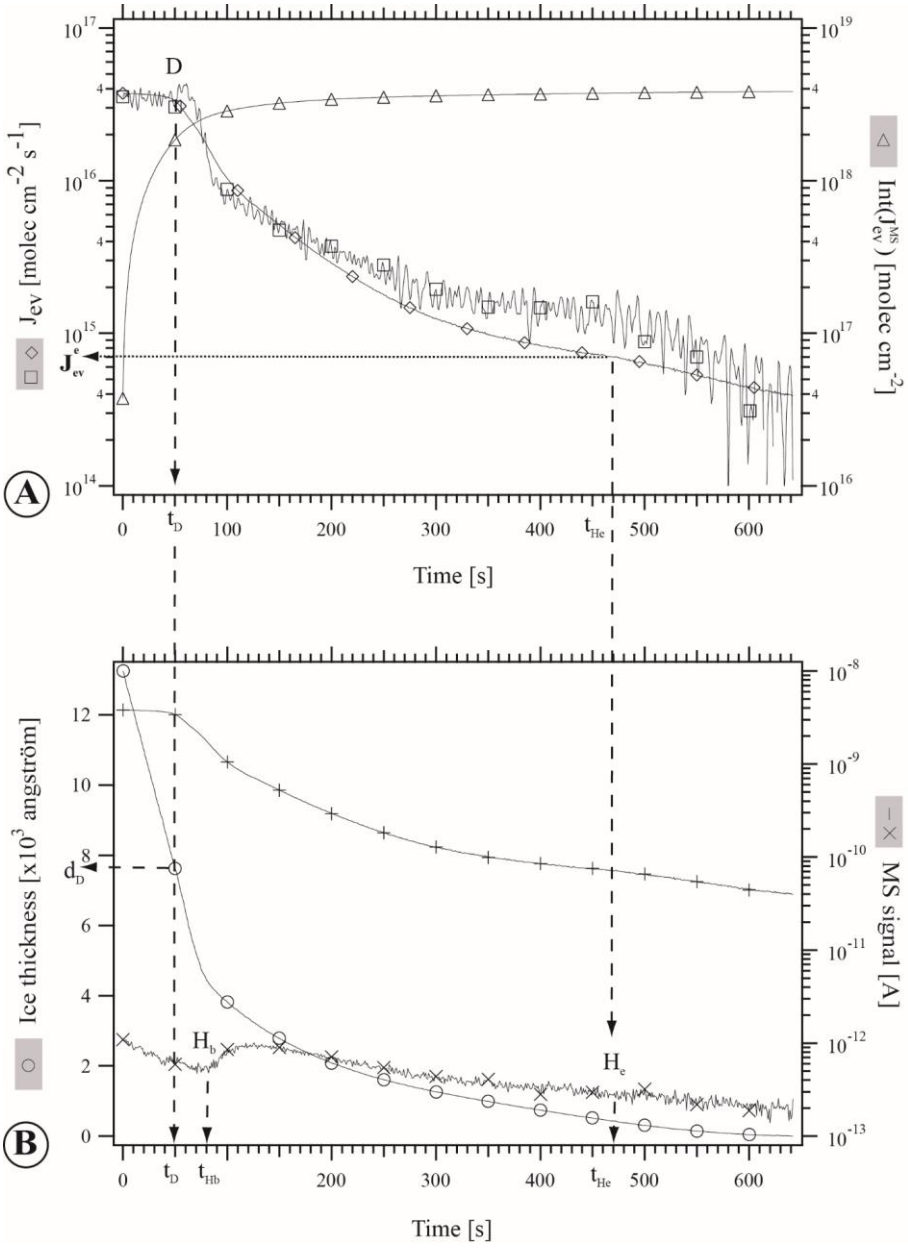
D
A
B
Time [s]
Time [s]
Ice thickness [x10^3 angström]
MS signal [A]
Int(J_ev^MS) [molec cm^-2]
J_ev [molec cm^-2 s^-1]
t_D
t_Hb
t_He
H_b
H_e
d_D

Figure 2

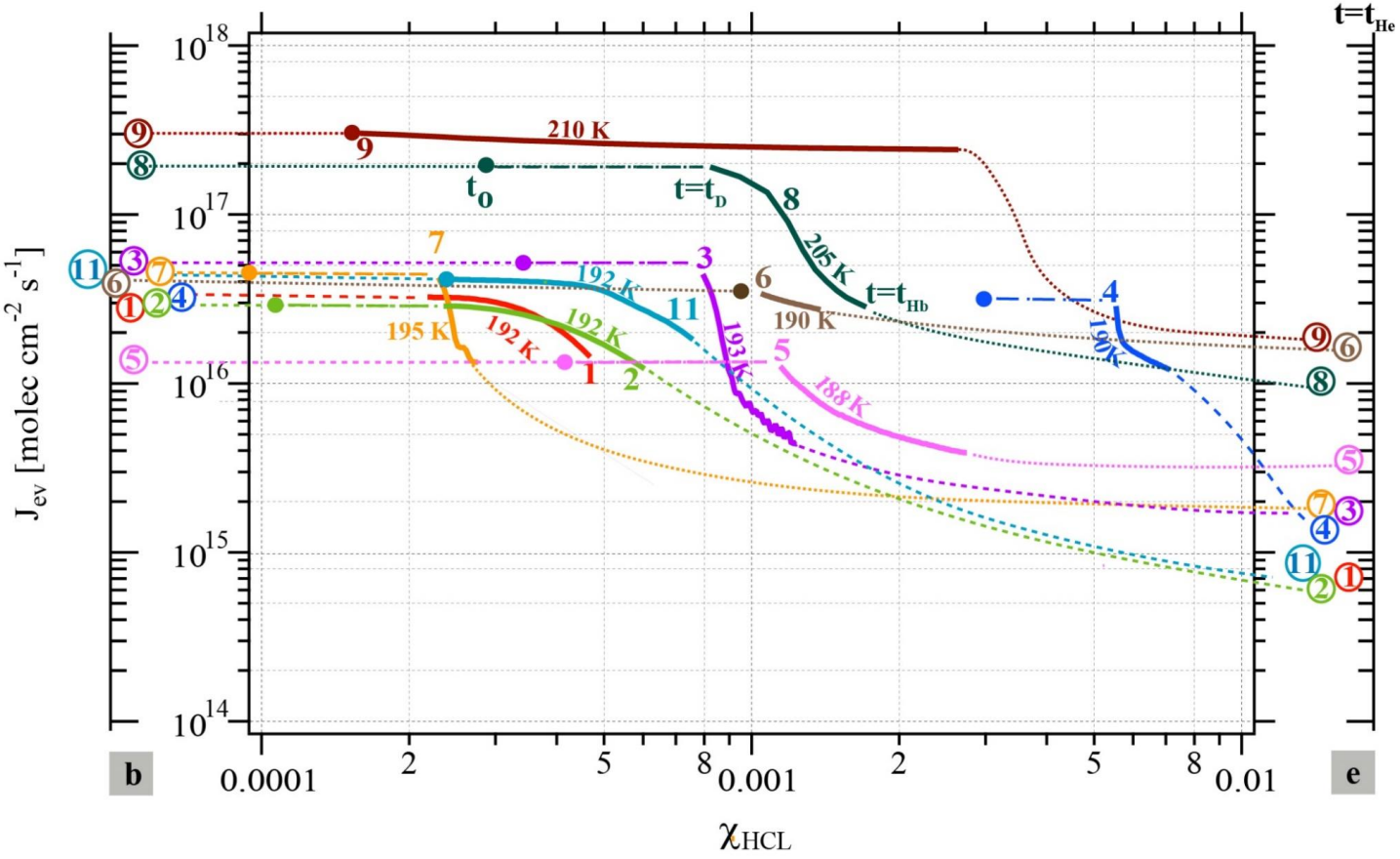
t=t_He
J_ev [molec cm^-2 s^-1]
χ_HCL
b
e
0.0001
0.001
0.01
210 K
205 K
192 K
195 K
190 K
193 K
188 K
t_o
t=t_D
t=t_Hb

Figure 3

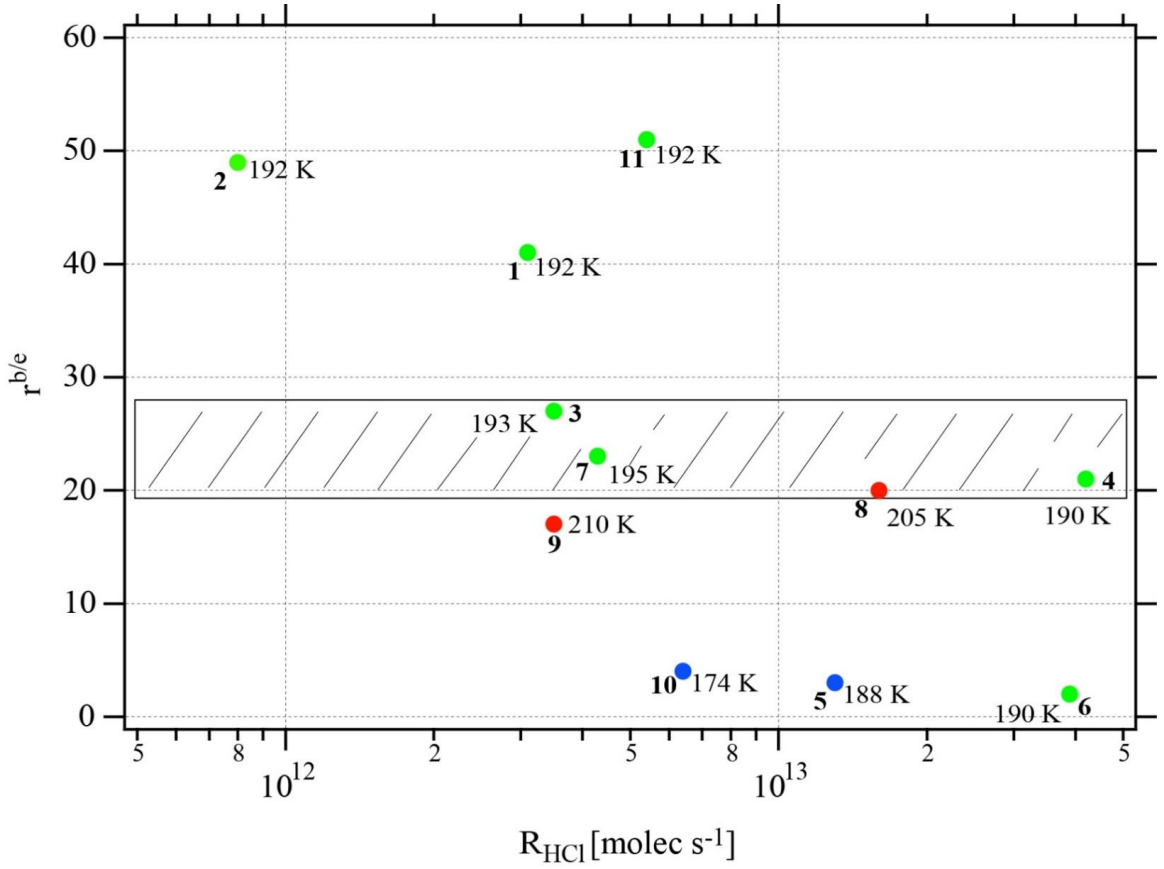
60
50
40
30
20
10
0
r b/e
2 192 K
11 192 K
1 192 K
193 K 3
7 195 K
4
8 205 K
190 K
9 210 K
10 174 K
5 188 K
190 K 6
5
8
10^12
2
5
8
10^13
2
5
R_HCl [molec s^-1]

Figure 4

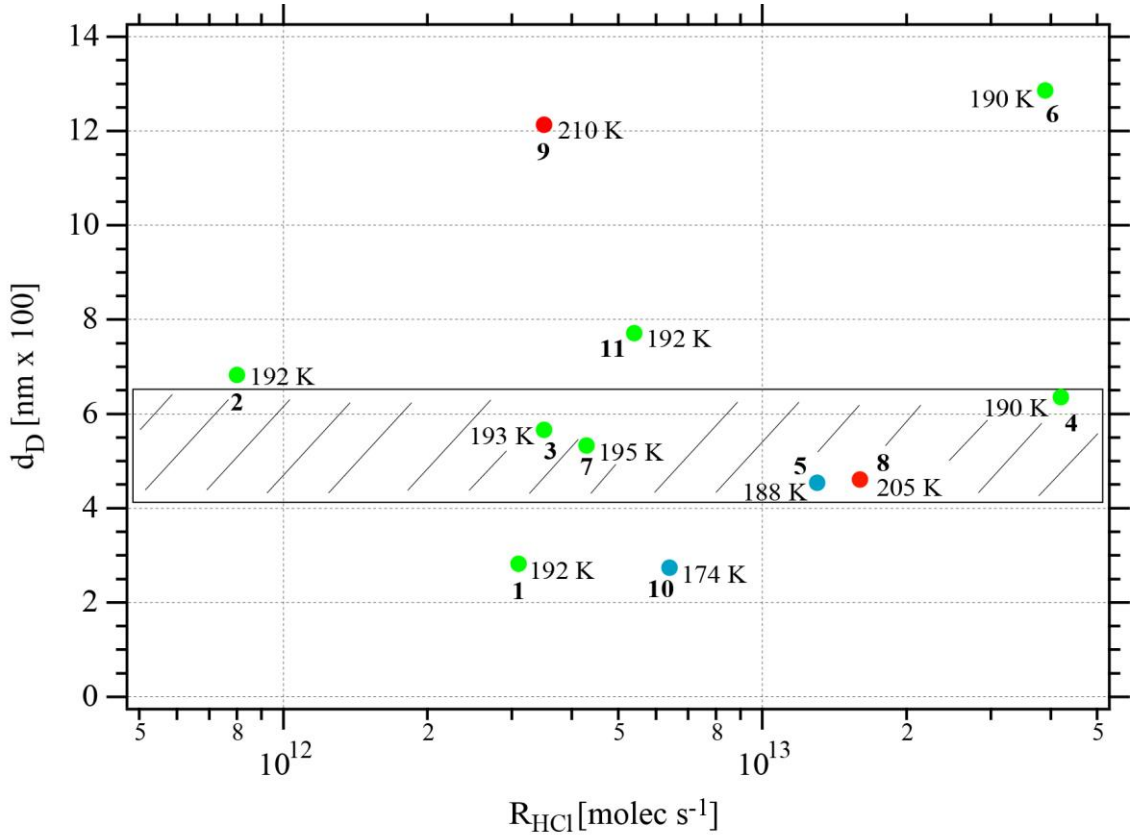
14
12
10
8
6
4
2
0
$d_D$ [nm x 100]
210 K
9
190 K
6
192 K
11
192 K
2
193 K
3
195 K
7
190 K
4
188 K
5
205 K
8
192 K
1
174 K
10
5
8
$10^{12}$
2
5
8
$10^{13}$
2
5
$R_{HCl}$[molec $s^{-1}$]

## APPENDIX A: Figures A1, A2, A3 and A4, Table A1

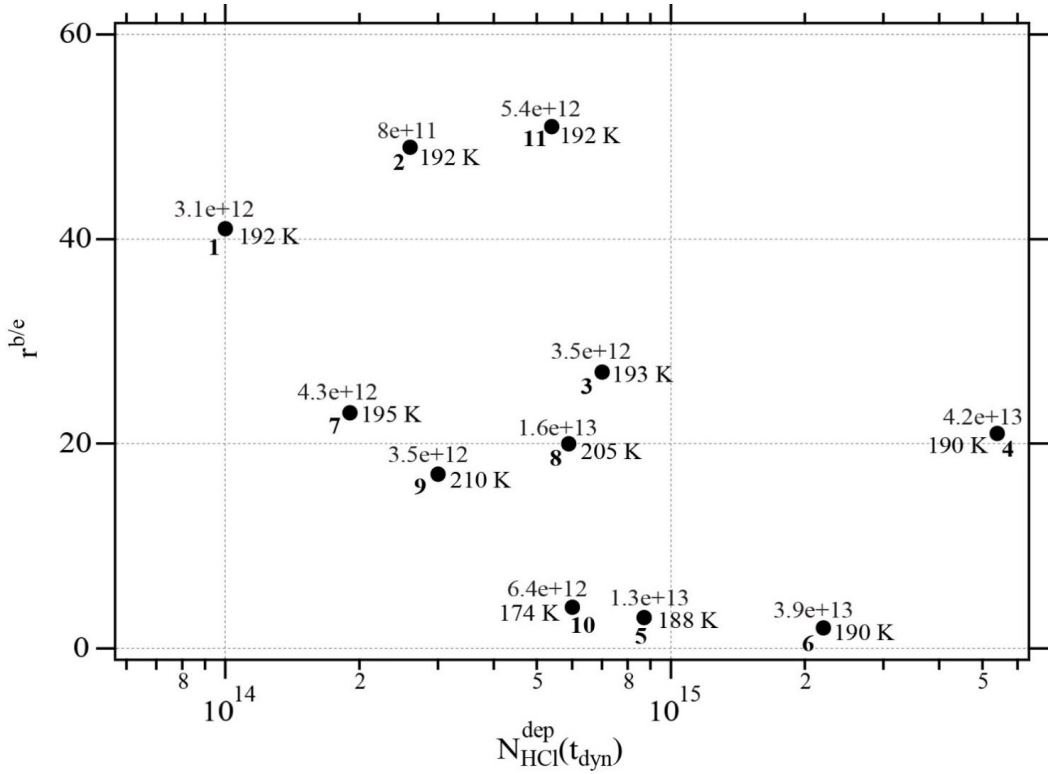


Figure A1: Synopsis of the dependence of the evaporation range parameter, $r^{b/e}$, on the number of adsorbed HCl, $N_{HCl}^{dep}$, adsorbed on ice for temperatures between 188 and 210 K. each point is marked with the deposition rate of HCl molecules in molec $s^{-1}$ on the ice film, the temperature of the ice film and the experiment running number (bold) referring to Table 2.

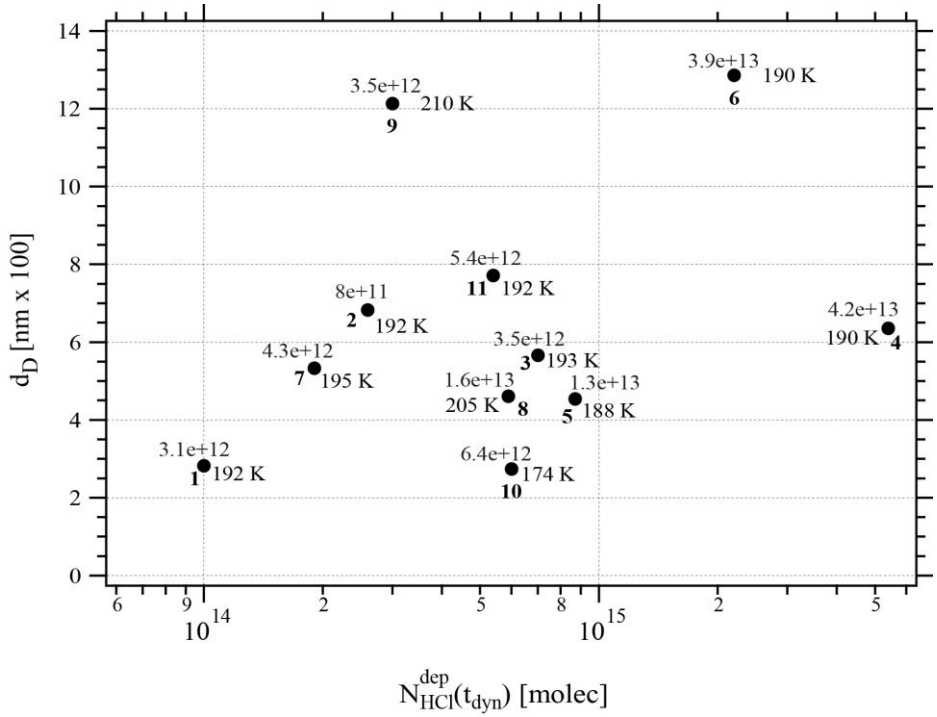


Figure A2: Synopsis of the dependence of the remaining thickness $d_D$ on the number of adsorbed HCl, $N_{HCl}^{dep}$, dispensed on ice for temperatures between 188 and 210 K. Each point is marked with the deposition rate of HCl in molec $s^{-1}$ on the ice film, the temperature of the ice film and the experiment running number (bold) referring to Table 2.

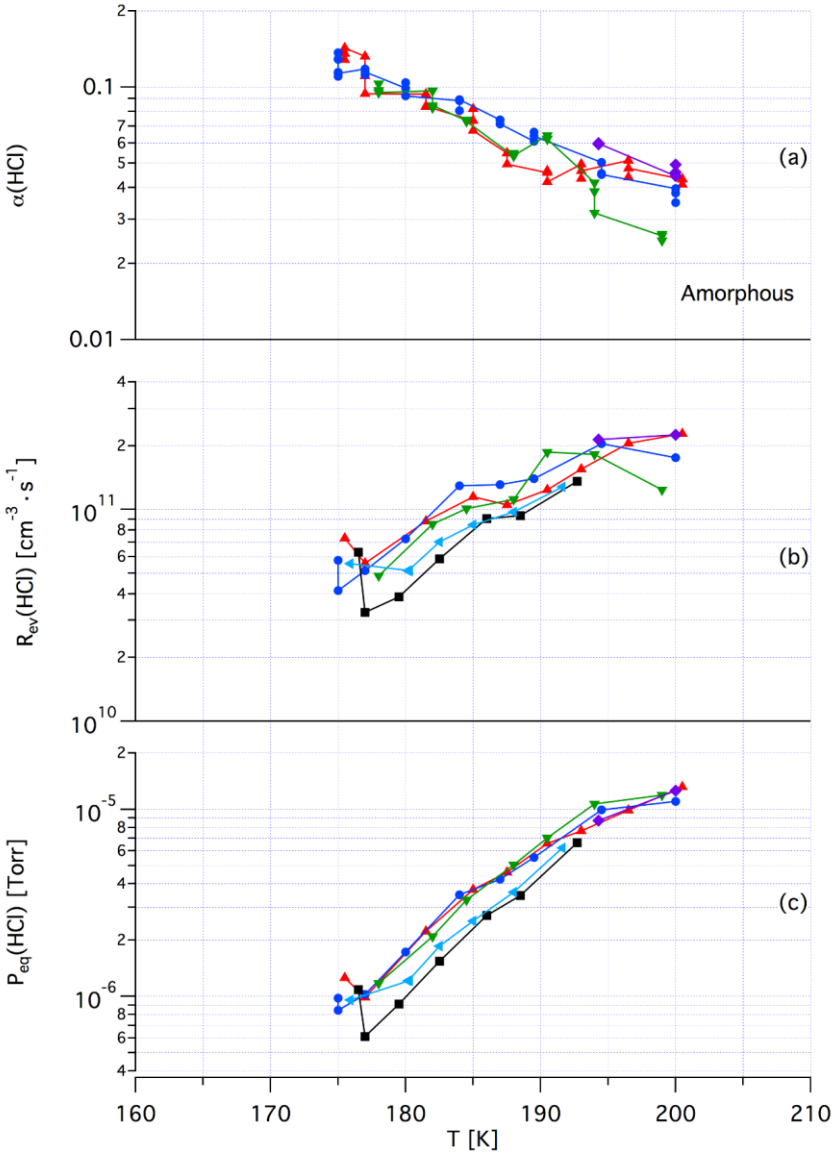


Figure A3: Synopsis of kinetic and thermodynamic results for an amorphous $H_2O$/HCl mixture using HCl as a probe gas. The symbols/colors used correspond to different experimental runs and the graphs show the scatter of the individual measurements within a series. Original data are published in Iannarelli, R. and Rossi, M.J. Atmos. Chem. Phys. **2014**, *14*, 5183–5204.

**Formatted:** Font: Bold

**Formatted:** Font: Italic

**Deleted:** , 2014

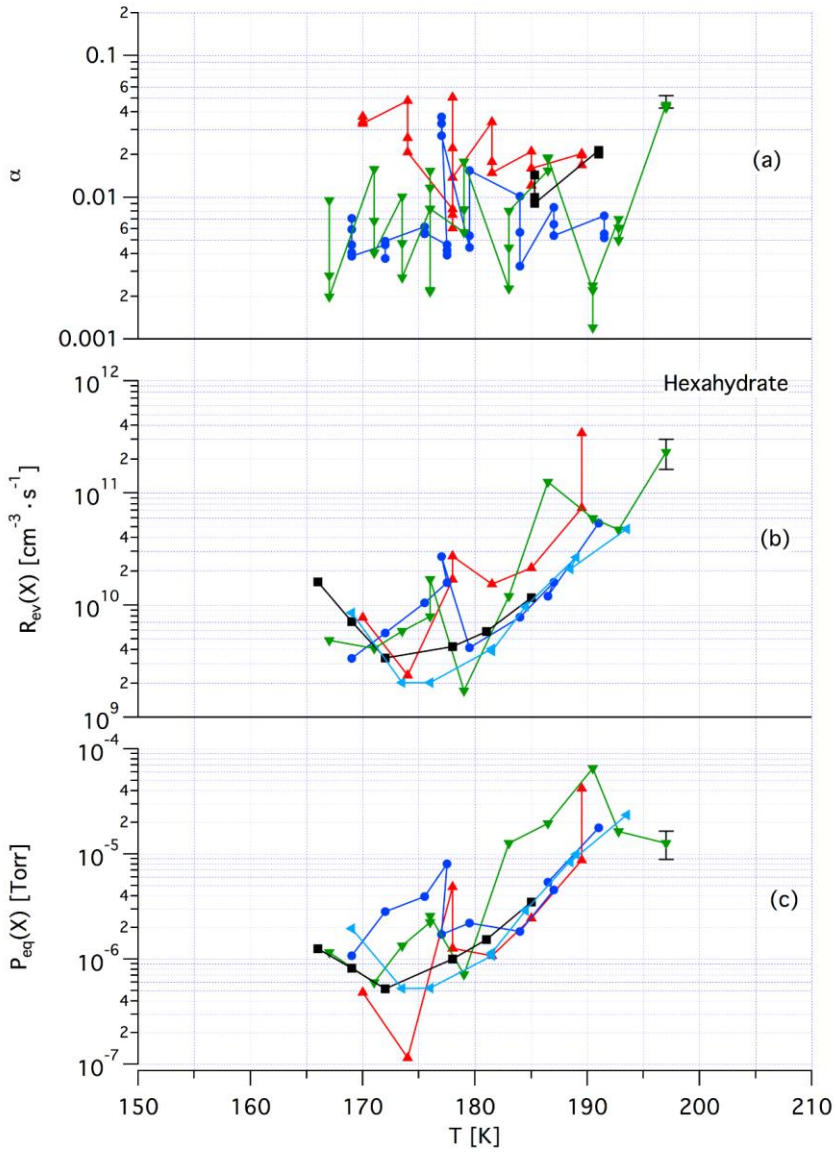


Figure A4: Synopsis of kinetic and thermodynamic results for crystalline HCl hexahydrate (HH) using X = HCl as a probe gas. The symbols/colors used correspond to different experimental runs and the graphs show the scatter of the individual measurements within a series. Original data are published in Iannarelli, R. and Rossi, M.J. Atmos. Chem. Phys. **2014**, *14*, 5183–5204.

**Formatted:** Font: Bold

**Formatted:** Font: Italic

**Deleted:** , 2014

**Table A1: Brief Summary of the Amount of a Molecular Monolayer (Coverage) of HCl adsorbed on $H_2O$ ice**

| Coverage / (molecule $cm^{-2}$) | Temperature / K | Bibliographic Reference |
|---|---|---|
| $5.0\ 10^{15}$ | 200 | Hanson, D. R., Mauersberger, K., HCl/$H_2O$ Solid Phase Vapor Pressures and HCl Solubility in Ice, J. Phys. Chem. **1990**, *94*, 4700–4705. |
| $1.0\ 10^{15}$ | 200 | Abbatt, J.P.D., Beyer, K. D., Fucaloro, A. F., McMahon, J. R., Wooldridge, P. J., Zhang, R., Molina, M. J., Interaction of HCl vapor with water ice: implications for the stratosphere, J. Geophys. Res. **1992**, *97*, 15819–15826. |
| $(2.0 – 3.0)\ 10^{14}$ | 191 | Hanson, D., Ravishankara, A.R., Investigation of the Reactive and Nonreactive Processes Involving $ClON0_2$ and HCl on Water and Nitric Acid Doped Ice, J. Phys. Chem. **1992**, *96*, 2682-2691. |
| $1.15\ 10^{15}$ | 183 | Foster, K. L., Tolbert, M. A., George, S. M., Interaction of HCl with Ice: Investigation of the Predicted Trihydrate, Hexahydrate, and Monolayer Regimes, J. Phys. Chem. A, **1997**, *101*, 4979–4986. |
| $2.5\ 10^{14}$ | 208 | Interaction of $HNO_3$ with water-ice surface at temperatures of the free troposphere, Abbatt, J.P.D., Geophys Res. Lett. **1997**, *24*, 1479-1482. |
| $3.1\ 10^{14}$ | 185 | Flückiger, B., Thielmann, A., Gutzwiller, L., Rossi, M. J., Real time kinetics and thermochemistry of the uptake of HCl, HBr and HI on water ice in the temperature range 190 to 210 K, Ber. Bunsenges. Phys. Chem. **1998**, *102*, 915–928. |
| $(1.1 \pm 0.6)\ 10^{14}$ | 201 | Lee, S.-H., Leard, D. C., Zhang, R., Molina, L. T., Molina, M. J., The HCl + $ClONO_2$ reaction on various water ice surfaces, Chem. Phys. Lett. **1999**, *315*, 7–11. |
| $(2.0 \pm 0.7)\ 10^{14}$ | 2001 | Hynes, R. G., Mössinger, J. C., Cox, R. A.: The interaction of HCl with water-ice at tropospheric temperatures, Geophys. Res. Lett. **2001**, *28*, 2827–2830. |
| $1.7\ 10^{14}$<br>$1.3\ 10^{14}$<br>$6.7\ 10^{13}$ | 190<br>200<br>210 | Flückiger, B., Rossi, M.J., Common Precursor Mechanism for the Heterogeneous Reaction of $D_2O$, HCl, HBr, and HOBr with Water Ice in the Range 170-230 K: Mass Accommodation Coefficients on Ice, J. Phys. Chem. A **2003**, *197*, 4103-4115. |
| $2.3$ to $2.7\ 10^{14}$ | 180 to 200 | Henson, B. F., Wilson, K. R., Robinson, J. M., Noble, C. A., Casson, J. L., Worsnop, D. R.: Experimental isotherms of HCl and $H_2O$ ice under stratospheric conditions, Connections between bulk and interfacial thermodynamics, J. Chem. Phys. **2004**, *121*, 8486– 8499. |

Deleted: ,
Formatted: Font: Bold
Deleted: , 1990
Formatted: Font: Italic
Formatted: Font: Bold
Formatted: Font: Italic
Deleted: , 1992
Formatted: Font: Bold
Formatted: Font: Italic
Deleted: , 1992
Formatted: Font: Bold
Formatted: Font: Italic
Deleted: , 1997
Deleted: , 1997
Formatted: Font: Bold
Formatted: Font: Italic
Formatted: Font: Bold
Formatted: Font: Italic
Deleted: , 1998
Formatted: Font: Bold
Formatted: Font: Italic
Deleted: , 1999
Formatted: Font: Bold
Formatted: Font: Italic
Deleted: , 2001
Formatted: Font: Bold
Formatted: Font: Italic
Deleted: , 2003
Formatted: Font: Bold
Formatted: Font: Italic
Deleted: , 2004